FORMATION CROSS SECTION OF H_2^+ IN THE REACTION OF FAST PROTONS AND METHANE

by

John Thomas Mitchell, Jr.

United States
Naval Postgraduate School

THESIS

FORMATION CROSS SECTION OF H_2^+ IN THE REACTION OF FAST PROTONS AND METHANE

by

John Thomas Mitchell, Jr.

September 1970

Formation Cross Section of H_2^+ in the Reaction of Fast Protons and Methane

by

John Thomas Mitchell, Jr.
Lieutenant, United States Navy
B.S., Rice University, 1964

Submitted in partial fulfillment of the
requirements for the degree of

MASTER OF SCIENCE IN PHYSICS

from the

NAVAL POSTGRADUATE SCHOOL
September 1970

ABSTRACT

The cross section for the formation of H_2^+ in the reaction $\underline{H}^+ + CH_4 \rightarrow \underline{H}_2^+ + CH_3$ was measured at scattering angles of 43° to 49.5° and incident proton energies of 70, 100 and 150 eV. For 150 eV the cross section showed no peak as a function of scattering angle. For 70 and 100 eV a pronounced peak was observed around a scattering angle of 46°. The position of the peak tended toward the theoretical limit of 46.9° as the incident proton energy was increased. The total cross section was 2.2×10^{-21} cm^2 at 70 eV and 8.1×10^{-22} at 100 eV. The angular position of the peak, the magnitude and the energy dependence of the cross section were in accordance with the classical theory of ion-molecule rearrangement collisions proposed by Bates, Cook and Smith.

TABLE OF CONTENTS

Blank

Page 4

LIST OF FIGURES

ACKNOWLEGEMENTS

I wish to express by appreciation to my thesis advisors Dr. Otto Heinz and Dr. Edward Milne for their encouragement, vast experience, and confidence. I am also grateful to Dr. Charles Cook of Stanford Research Institute for his invaluable assistance. In particular, my special thanks is directed to Mr. Thomas Maris of the Naval Postgraduate School, Physics Department Technicial Staff for his constant assistance, great technical skill and his apparently inexhaustable patience.

I owe a great deal to my fiance Judy, whose love and strong right foot directly contributed to the successful conclusion of this project.

I would like to dedicate this work to the memory of my longtime friend and associate, LT William Latta, USN.

Blank

page 8

I. INTRODUCTION

Modern quantum theory has as one of its major accomplishments the accurate and detailed description of complex atomic and molecular interactions. However it is evident in practice that the mathematical complexity involved in modern quantum theory is such that only the most simple case can be treated rigorously. Various approximations are employed to simplify these mathematical computations. It then becomes of primary interest to know the accuracy, nature and range of applicability of these approximations. These questions are normally answered most satisfactorily by comparison of the predictions of a specific approximate calculation and experimental results.

It is the purpose of this paper to present the results of measurements which verify the predictions of a classical theory of ion-molecule rearrangement collisions at high impact energies as proposed by Bates, Cook and Smith [1]. This theory uses an impulse type approximation to obtain the cross section for the capture of a light atom or ion from a target molecule by a fast moving projectile. Applying this theory to the reaction:

$$\underline{H}^+ + CH_4 \rightarrow \underline{H}_2^+ + CH_3 \qquad (1)$$

the cross section is predicted to show a sharp peak at 46.9^o with an upper limit on the magnitude of the cross section of 1.4×10^{-20} cm^2 at 100 eV incident proton energy. The theory also

predicts that the magnitude of the proton energy should decrease rapidly with increasing incident proton energies, approaching an energy dependence of $E^{-5.5}$ asymptotically at energies above 500 eV. the range of validity at the theory extends from about 50 to 800 eV when applied to reaction (1).

Our measurements were carried out at energies of 70, 100 and 150 eV including angles of scattering from 43° to 49.5°. We found essential agreement between the predictions of the theory and the experimental data and previous experimental data. This indicates that the classical impulse approximation proposed by Bates, Cook and Smith is a valid model for reaction (1) in the energy range considered.

II. THEORY

A. CLASSICAL THEORY OF ION-MOLECULE REARRANGEMENT COLLISIONS

Bates, Cook and Smith [1] have proposed a classical theory of ion-molecule rearrangement collisions at energies greater than 50 electron volts. The impact energies are assumed to be high enough so that polarization forces and chemical binding energies of the colliding molecules can be ignored. The theory applies to various ion-molecule rearrangement reactions of the type

$$\underline{X'X_i} + YZ_kZ' \rightarrow \underline{X'} + \underline{X_iY} + (\underline{Z_k} + Z') \qquad (1)$$

where X_i and Y are simple atoms or ions. The bar is used to indicate which ions are fast in the laboratory coordinate system. An example of a rearrangement reaction of this type is

$$\underline{H^+} + CH_4 \rightarrow \underline{H_2^+} + CH_3 \ . \qquad (2)$$

The basic assumption made by Bates, Cook and Smith, is that process (1) may be described by a classical impulse approximation similar to that developed by Thomas [2], for the description of electron capture, where each composite system is regarded as a loose cluster of atoms and ions. (Eg $H_2^+ = H + H^+$ and $CH_4 = C + 3H + H$).

According to this model, we can consider the reaction to occur in the following manner: consider a particle of mass M_1 moving with velocity $\vec{v}_1$ through molecules of loosely bound

particles of mass M_2 and M_k. Figure 1 shows the sequence of collisions that lead to the capture of M_2 by M_1. First mass M_1 collides with mass M_2. This causes M_1 to be scattered at an angle θ_1' and velocity $\vec{v}_1'$ while M_2 recoils at an angle θ_2' with velocity $\vec{v}_2'$. Mass M_2 then suffers a second binary collision with mass M_k. This causes M_2 to be scattered at an angle θ_2'' with velocity $\vec{v}_2''$.

$$\left.\begin{array}{l}\text{Now if: (a) } \theta_2'' \simeq \theta_2' + \theta_1' \\ \\ \text{And if: (b) } v_1' \simeq v_2''\end{array}\right\} \quad \text{or } \vec{v}_1' = \vec{v}_2'' \qquad (3)$$

then masses M_1 and M_2 may have a relative energy of motion below that required for separation, and so, the two particles may combind and proceed on as one. If the particle with mass M_1 is a composite particle then its disruption can be avoided if

$$\vec{v}_1' \simeq \vec{v}_1. \qquad (4)$$

In the particular case of:

$$M_2 = M_1 << M_k$$

condition (3) is satisfied if $\theta_1' \simeq 45^\circ$ and $\theta_2'' \simeq 90^\circ$ (see Section B of this Chapter), but then condition (4) is violated. In the case of the reaction:

$$\underline{H}^+ + CH_4 \rightarrow \underline{H}_2^+ + CH_3$$

where $M_1 = M_{H+}$, $M_2 = M_H$ and $M_k = M_{CH_3}$, the violation of condition (4) is not relevant since M_1 is not a composite particle.

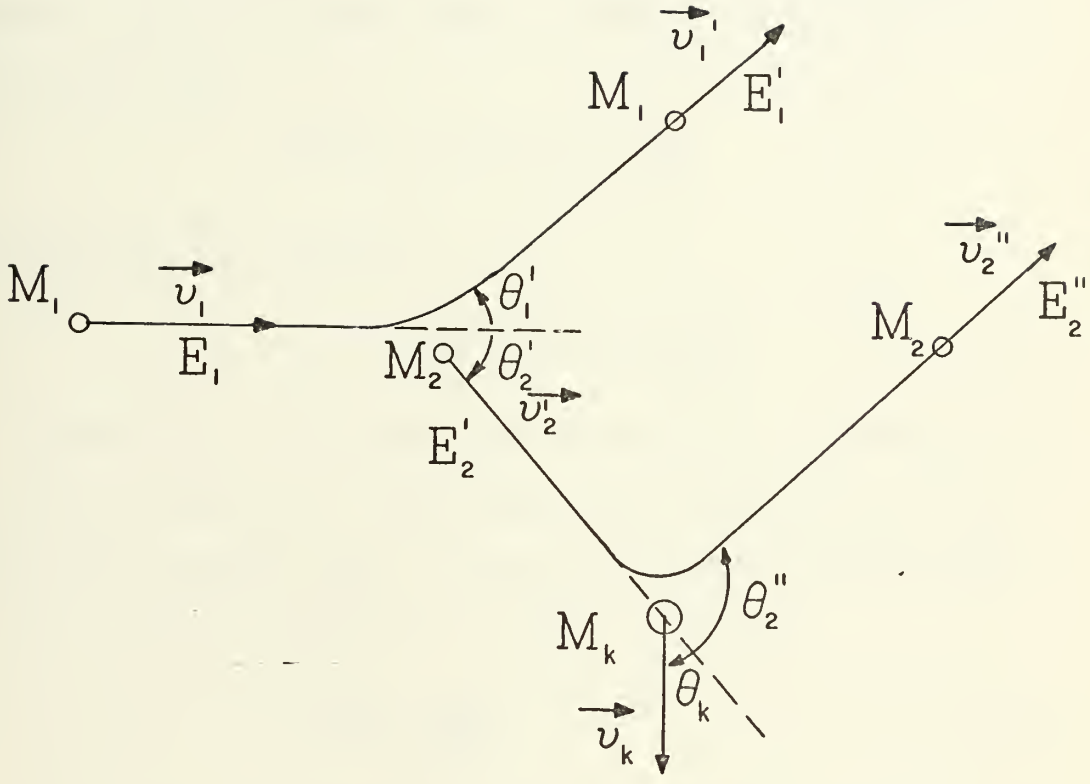

FIGURE 1 THE CAPTURE MECHANISM

Consider now, the first binary collision between M_1 and M_2 as shown in Figure 2. The probability of scattering M_2 into the solid angle $d\Omega(\theta_2')$ with velocity between $\vec{v}_2'$ and $\vec{v}_2' + d\vec{v}_2'$ is:

$$q = \sigma_{12}(\theta_2')\ d\Omega(\theta_2') \tag{5}$$

where $\sigma_{12}(\theta_2')$ is the appropriate differential scattering cross section. Since the solid angle is the cone of semi-angle θ_2' within $d\theta_2'$ then:

$$d\Omega(\theta_2') = 2\pi \sin\theta_2'\ d\theta_2'$$

and equation (5) becomes:

$$q = 2\pi\ \sigma_{12}(\theta_2')\ \sin\theta_2'\ d\theta_2' \ . \tag{6}$$

Consider now, the second binary collision between M_2 and M_k as shown in Figure 3. The probability of M_2 having an impact parameter between ρ and $\rho + d\rho$ and an azimuthal angle between ψ and $\psi + d\psi$ at a distance r from M_k is given by

$$p = \rho d\rho\ \frac{d\psi}{4\pi r^2} \tag{7}$$

where r is the M_2-M_k equilibrium internuclear separation. But particles incident on M_k with impact parameter ρ and azimuthal angle ψ are scattered into the solid angle $dr(\theta_2'')$ at θ_2''.

Hence: $$\rho d\rho = \sigma_{2k}\ (\theta_2'')\ d\Omega(\theta_2'')$$

where $\sigma_{2k}(\theta_2'')$ is the appropriate differential scattering cross section.

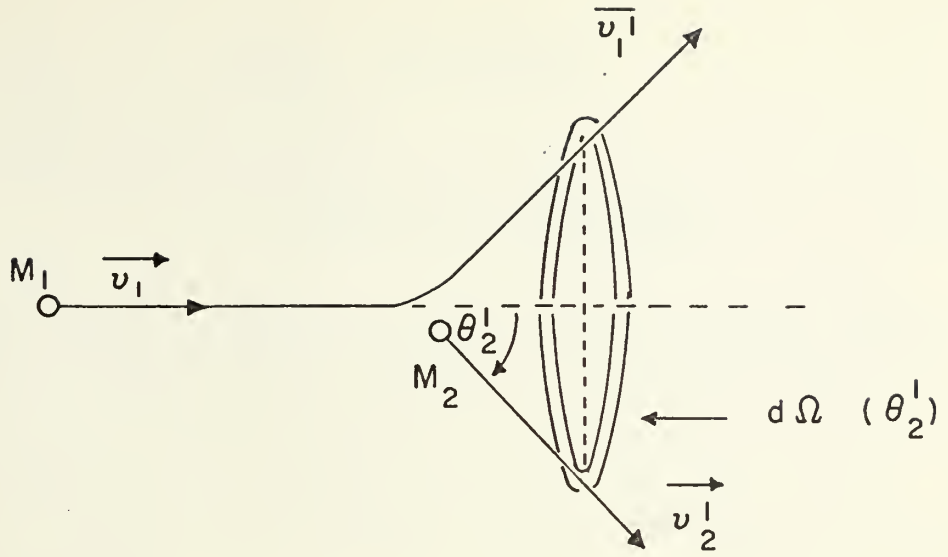

FIGURE 2. THE FIRST BINARY COLLISION

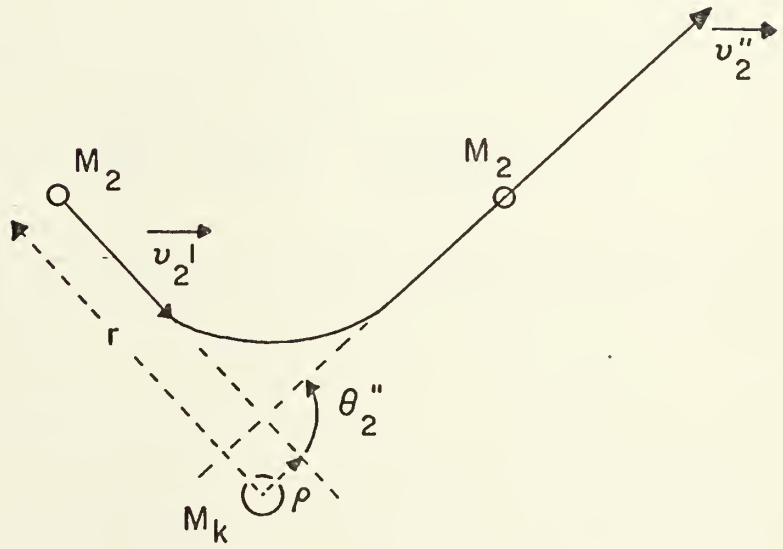

FIGURE 3. THE SECOND BINARY COLLISION

But: $$d\Omega(\theta_2'') = \sin\theta_2''\, d\theta_2''$$

Hence equation (7) becomes:

$$p = \sigma_{2k}(\theta_2'') \sin\theta_2''\, d\theta_2'' \frac{d\psi}{4\pi r^2} . \qquad (8)$$

Now, for M_1 to capture M_2, $\vec{v}_1' - \vec{v}_2''$, the relative velocity of M_1 and M_2, must be contained within a volume of velocity space determined by D, the mutual affinity of these two systems. In the high velocity limit, Bates, Cook and Smith [1], state this requirement as:

$$(v_2'')^2 \sin\theta_2''\, d\theta_2''\, d\psi\, dv_2'' = \lambda\frac{4}{3}\pi\left(\frac{2D}{\mu}\right)^{3/2} \qquad (9)$$

where $\lambda = \frac{1}{2}$ and $\mu = \frac{1}{2}M_2$ in the case $M_2 = M_1 < M_k$. (10)

Substituting equation (9) into equation (8) we get

$$p = \frac{\sigma_{2k}(\theta_2'')}{3r^2}\left(\frac{2D}{\mu}\right)^{3/2} \frac{\lambda}{(v_2'')^2 dv_2''} . \qquad (11)$$

Now, the capture cross section arising from the M_1-M_2-M_k sequence of binary collisions is:

$$Q(M_1\text{-}M_2\text{-}M_k) = \gamma\, pq \qquad (12)$$

where γ is a dimensionless factor, less than, or equal to unity, which allows for the fact that M_1 and M_2 may approach each other such that in the resulting state, the affinity is less then that assumed.

Substituting equations (6) and (11) into (12) one gets:

$$Q(M_1\text{-}M_2\text{-}M_k) = \gamma\lambda \frac{2\pi\, \sigma_{12}(\theta_2')\sigma_{2k}(\theta_2'')}{3r^2} \sin\theta_2'\, d\theta_2' \left(\frac{2D}{\mu v_2''}\right)^{3/2} \frac{v_2''}{dv_2''} . \quad (13)$$

Changing from Lab. to Center of Mass coordinates, one gets for the case of $M_1 = M_2 << M_k$

$$Q(M_1\text{-}M_2\text{-}M_k) = \gamma \frac{16\pi\, \bar{\sigma}_{12}(90^\circ)\, \bar{\sigma}_{2k}(90^\circ)}{3r^2} \left(\frac{2D}{M_2 v_1^2}\right)^{3/2} \quad (14)$$

where $\bar{\sigma}_{12}$ and $\bar{\sigma}_{2k}$ denote the differential scattering cross sections in the center of mass coordinate systems. This differential cross section is at an energy of relative motion of $\frac{1}{4}M_2 v_1^2$ and the affinity D is at an M_2-M_k internuclear distance of $\sqrt{2}\,r$. To obtain the total cross section for capture, Q, one now sums over all binary collision sequences which lead to the same final capture process. For example, the total cross section for process (2) is

$$Q = 4Q(H^+\text{-}H - C) \quad + 4Q\,(H\text{-}H^+ - C).$$

This represents the two possible collision sequences shown below:

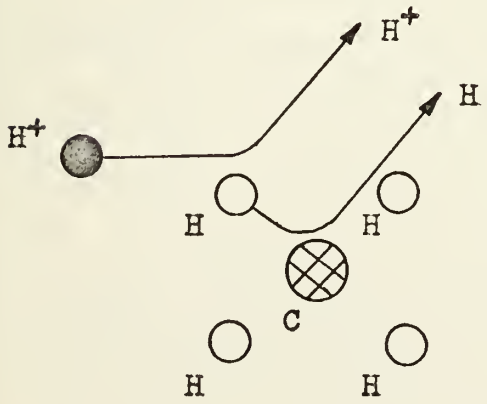

The (H^+- H - C) Sequence

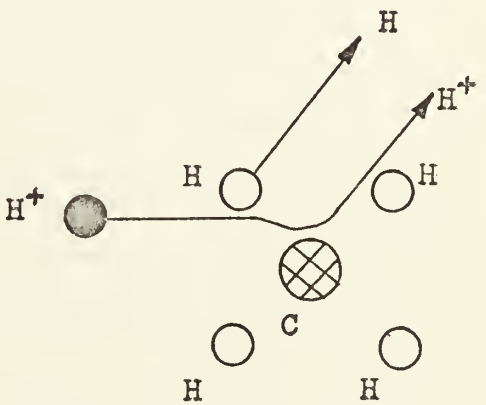

The (H- H^+ - C) Sequence

Solution of Rutherford's expression for the differential scattering cross section when v_1 is high enough for the atomic field to be Coulombic, shows that:

$$Q(M_1\text{-}M_2\text{-}M_k) \sim v_1^{-11} \quad . \tag{15}$$

The range of validity of (14) does not extend indefinitely as v_1 increases. Two requirements must be satisfied:

(i) The De Broglie wavelength limitations,

(ii) The Heisenberg uncertainty relations.

Bates, Cook and Smith [1], computed the required differential scattering cross sections $\bar{\sigma}_{12}(90^\circ)$ and $\bar{\sigma}_{2k}(90^\circ)$ using classical methods and the analytic representation of the relevant Hartree potentials as given by Byatt [3]. From the results of these computations listed in Reference 1, the cross section for the rearrangement reaction:

$$\underline{H}^+ + CH_4 \rightarrow \underline{H}_2^+ + CH_3$$

is determined to be as shown in Figure 4.

B. THE $\underline{H}^+ + CH_4 \rightarrow \underline{H}_2^+ + CH_3$ REACTION KINETICS

The rearrangement mechanism for the reaction is shown in Figure 1, where M_1 represents the H^+, M_2 the H and M_k represents the CH_3. To determine the exact value of the scattering angle θ_1' one has to consider the kinematics of the arrangement process.

If the speed v_1 is assumed to be large enough so the binding energy of M_2 to M_k can be ignored, then the conservation laws can be applied in the usual manner.

FIGURE 4
PREDICTED CROSS SECTION FOR
$H^+ + CH_4 \longrightarrow H_2^+ + CH_3$
FROM BATES COOK SMITH'

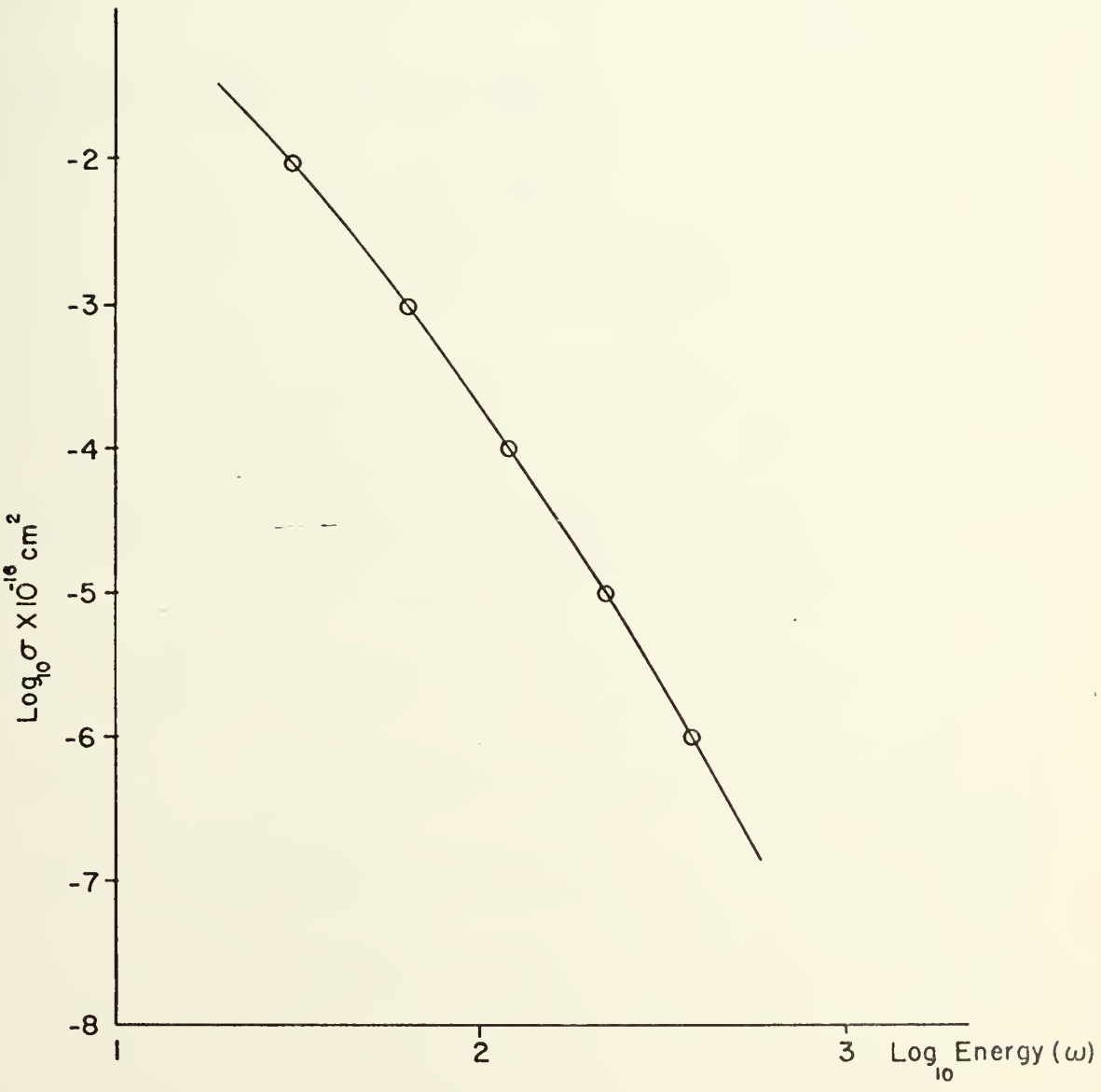

Consider the first binary collision of the reaction shown in Figure 1. From conservation of energy and momentum we have:

$$\tfrac{1}{2}M_1 v_1^2 = \tfrac{1}{2}M_1 (v_1')^2 + \tfrac{1}{2}M_2 (v_2')^2 \tag{16}$$

$$M_1 v_1 = M_1 v_1' \cos \theta_1' + M_2 v_2' \cos \theta_2' \tag{17}$$

$$0 = M_1 v_1' \sin \theta_1' - M_2 v_2' \sin \theta_2' \tag{18}$$

Now: $M_1 = M_2 = M_H$

Hence: the above equations become

$$v_1^2 = (v_1')^2 + (v_2')^2 \tag{19}$$

$$v_1 = v_1' \cos \theta_1' + v_2' \cos \theta_2' \tag{20}$$

$$0 = v_1' \sin \theta_1' - v_2' \sin \theta_2' \ . \tag{21}$$

Now θ_2' can be eliminated between (20) and (21) by rearranging, squaring, and adding the two equations to yield:

$$v_1^2 + (v_1')^2 - 2v_1 v_1' \cos \theta_1' = (v_2')^2 .$$

But from (19): $(v_2')^2 = v_1^2 - (v_1')^2$

Thus: $v_1^2 + (v_1')^2 - 2v_1 v_1' \cos \theta_1' = v_1^2 - (v_1')^2$

Hence: $(v_1')^2 = v_1 v_1' \cos \theta_1'$

$$\therefore v_1' = v_1 \cos \theta_1' \tag{22}$$

Substituting equation (22) back into equation (19) we get:

$$v_1^2 = v_1^2 (\cos \theta_1')^2 + (v_2')^2$$

or:

$$v_1^2 (1-\cos^2 \theta_1') = (v_2')^2$$

$$\therefore v_2' = v_1 \sin \theta_1' \ . \qquad (23)$$

Equations (22) and (23) give us v_1' and v_2' in terms of v_1 and θ_1'. Now we wish to obtain v_1' and v_2' in terms of v_1 and θ_2'. Thus we arrange equation (20) and (21) such that when we square and add them, we eliminate θ_1' and so obtain:

$$v_1^2 + (v_2')^2 - 2v_1 v_2' \cos \theta_2' = (v_1')^2 \ .$$

But from (19) we have: $(v_1')^2 = v_1^2 - (v_2')^2$

Thus: $$v_1^2 + (v_2')^2 - 2v_1 v_2' \cos \theta_2' = v_1^2 - (v_2')^2$$

Hence: $$v_2' = v_1 \cos \theta_2' \ . \qquad (24)$$

Substituting equation (24) back into equation (19) gives:

$$v_1^2 = (v_1')^2 + v_1^2 \cos^2 \theta_2'$$

or:

$$v_1^2(1-\cos^2\theta_2') = (v_1')^2$$

$$\therefore v_1' = v_1 \sin \theta_2' \ . \qquad (25)$$

Consider now, the second binary collision. Again ignoring the binding energies we can write the conservation of energy and momentum equations as:

$$\tfrac{1}{2} M_2(v_2')^2 = \tfrac{1}{2} M_2(v_2'')^2 + \tfrac{1}{2} M_k v_k^2 \qquad (26)$$

$$M_2 v_2' = M_2 v_2'' \cos \theta_2'' + M_k v_k \cos \theta_k \qquad (27)$$

$$0 = M_2 v_2'' \sin \theta_2'' - M_k v_k \sin \theta_k \qquad (28)$$

Now: $M_1 = M_2 = M_H$, $M_k = M_{CH_3}$

Thus the above three equations reduce to:

$$(v_2')^2 = (v_2'')^2 + \frac{M_k}{M_H} v_k^2 \qquad (29)$$

$$(v_2') = v_2'' \cos \theta_2'' + \frac{M_k}{M_H} v_k \cos \theta_k \qquad (30)$$

$$0 = v_2'' \sin \theta_2'' - \frac{M_k}{M_H} v_k \sin \theta_k \ . \qquad (31)$$

As we are not interested in θ_k we can eliminate it by suitably rearranging equations (30) and (31) and then squaring and adding. Thus we get:

$$(v_2')^2 + (v_2'')^2 - 2v_2' v_2'' \cos \theta_2'' = \left(\frac{M_k}{M_H}\right)^2 v_k^2 \ . \qquad (32)$$

But from equation (29):

$$\frac{M_k}{M_H} v_k^2 = (v_2')^2 - (v_2'')^2 \ .$$

Thus (32) becomes:

$$(v_2')^2 + (v_2'')^2 - 2v_2'v_2'' \cos \theta_2'' = \frac{M_k}{M_H} (v_2')^2 - \frac{M_k}{M_H} (v_2'')^2$$

or

$$(v_2')^2 \left(1 - \frac{M_k}{M_H}\right) + (v_2'')^2 \left(1 + \frac{M_k}{M_H}\right) - 2\, v_2'v_2'' \cos \theta_2'' = 0 \ .$$

Multiplying through by:

$$\frac{M_H}{M_k + M_h}\left(\frac{1}{v_2'}\right)^2 \quad \text{yields:}$$

$$\frac{M_H - M_k}{M_H + M_k} + \left(\frac{v_2''}{v_2'}\right)^2 - 2\,\frac{v_2''}{v_2'}\left(\frac{M_H}{M_H + M_k}\right)\cos\theta_2'' = 0. \qquad (33)$$

Now, let: $a = \dfrac{M_H}{M_k + M_H}$ and $b = \dfrac{M_k - M_H}{M_k + M_H}$.

Then (33) becomes:

$$\left(\frac{v_2''}{v_2'}\right)^2 - 2\left(\frac{v_2''}{v_2'}\right) a \cos\theta_2'' - b = 0 \ . \qquad (34)$$

But now, for capture, we require that : $\theta_2'' \simeq \theta_1' + \theta_2'$

thus: $\cos\theta_2'' \simeq \cos(\theta_1' + \theta_2')$

ie., $\cos\theta_2'' \simeq \cos\theta_1' \cos\theta_2' - \sin\theta_1' \sin\theta_2'$ and using (24) and (25) to eliminate θ_2' we have:

$$\cos\theta_2'' \simeq \cos\theta_1'\left(\frac{v_2'}{v_1}\right) - \sin\theta_1'\left(\frac{v_1'}{v_1}\right) \ .$$

Hence equation (34) becomes:

$$\left(\frac{v_2''}{v_2'}\right)^2 - 2a\left[\frac{v_2''}{v_2'}\frac{v_2'}{v_1}\cos\theta_1' - \frac{v_2''}{v_2'}\frac{v_1'}{v_1}\sin\theta_1'\right] - b = 0$$

or: $$(v_2'')^2 - 2av_2'\left[\frac{v_2''v_2'}{v_1}\cos\theta_1' - \frac{v_2''v_1'}{v_1}\sin\theta_1'\right] - b(v_2')^2 = 0. \qquad (35)$$

But now, the second capture criteria is that: $v_2'' \simeq v_1'$.

But, from equation (22) we have: $v_1' = v_1 \cos \theta_1'$.

Hence, we require for capture: $v_2'' \simeq v_1 \cos \theta_1'$. (36)

Substituting equations (22) and (36) into (35) we get:

$$v_1^2 \cos^2 \theta_1' - 2av_2' [v_2' \cos^2\theta_1' - v_1 \sin \theta_1' \cos^2\theta_1'] - b(v_2')^2 = 0.$$

Using (23) to eliminate v_2' from this equation we get:

$$v_1^2 \cos^2 \theta_1' - b\, v_1^2 \sin^2 \theta_1' = 0.$$

Hence, for capture to occur we must have:

$$\tan \theta_1' = \sqrt{\frac{1}{b}} = \sqrt{\frac{M_k + M_H}{M_k - M_H}} \quad . \tag{37}$$

Now $M_k = M_{CH_3} = 15.03506$ and $M_H = 1.00797$ amu. Thus the angle at which capture occurs is

$$\theta_1' = 46.926^\circ \tag{38}$$

Hence we expect the capture cross section to show a pronounced peak at this angle. From Figure 4, the magnitude of the cross section is paredicted to be approximately 1.4×10^{-20} cm^2 if the energy of the incident proton beam is 100 eV.

C. THE RANGE OF VALIDITY OF THE CLASSICAL DESCRIPTION

A lower limit on the range of validity of the classical treatment of the rearrangement collision is imposed by the assumption made in the theoretical development that the energies

involved in the collision are much larger than the binding energies. Hence, when the energy of the incident proton beam E_1 is less than, or equal to about 10 times the binding energy, we expect the peak in the cross section to become less pronounced and more spread out. Thus the theory is valid when $E_1 \simeq 50$ eV.

An upper limit on the range of validity of the theory is determined by the two requirements:

(i) The Di Broghlie Wavelength λ of any particle must be much less than the smallest distance involved in the collision S.

Hence, we require $\lambda \ll S$ (39)

(ii) The uncertainty in energy introduced by specifying the transverse position of the proton must be much less than the binding energy of the final product. Now, from (29) we know the uncertainty in the proton position λ is less than the distance of closest approach S.

But we can write the uncertainty relation:

$$\Delta x \Delta p = \frac{\hbar}{2} \tag{40}$$

as $$S\Delta p >> \frac{\hbar}{2}$$

Thus $$\Delta p >> \frac{\hbar}{2S} \tag{41}$$

or $$\Delta E = \frac{\Delta p^2}{2M_H} >> \frac{\hbar^2}{8M_H S^2} . \tag{42}$$

We then demand that the binding energy D be greater than ΔE, or:

$$D >> \frac{\hbar^2}{8M_H S^2} . \tag{43}$$

To find what restrictions equations (39) and (43) place on the energy of the incident proton beam we have to relate the distance of closest approach S to the energy of the proton beam E_1. This can be done quite readily in the case of coulomb collisions. By considering the collisions to be coulomb it will be shown that:

$$S = \frac{C_1}{E_1}$$

and

$$\lambda = \frac{C_2}{\sqrt{E_1}}$$

where C_1 and C_2 are constants. Because S decreases faster than λ as E_1 increases, we see that equation (39) will indeed place an upper limit on the energy E_1.

In a coulomb collision the point of closest approach is yielded by solving the equation:

$$1 - \frac{b^2}{S^2} - \frac{\phi(S)}{U_1} = 0 \qquad (44)$$

(see equation 3-4-3 of Ref. 4)

U_1, the Center of Mass energy, can be expressed as $U_1 = \frac{1}{2} \mu v_{rel}^2$ where μ is the reduced mass and v_{rel} is the relative speed of approach. $\phi(S)$, the potential energy at the distance of closest approach, is:

$$\phi(S) = \frac{(Ze)(Z'e')}{S}$$

The impact parameter b is given by:

$$b = \frac{(Ze)(Z'e')}{\mu v_{rel}^2} \cot \frac{\Theta}{2} \qquad (45)$$

(see equation 3-8-8 of Ref. 4)

Where Θ is the Center of Mass scattering angle.

Now we have two collisions to consider:

(i) In the first binary collision (H^+ -H) we have (see Figure 1)

$$\Theta = 90^o, \ \mu = \frac{M_H}{2}, \ v_{rel} = v_1 \tag{46}$$

(ii) In the second binary collision (H - C) we have (see Figure 1)

$$\Theta \simeq \Theta_2'' = 90^o, \ \mu \simeq M_H, \ v_{rel} = v_2' \tag{47}$$

and since $E_2' \simeq \frac{1}{2} E_1$ we have $v_2' \simeq \frac{1}{\sqrt{2}} v_1$.

Making these substitutions in (45) we get:

$$b_{H^+ - H} = \frac{e^2}{E_1} \tag{48}$$

$$b_{H-C} = 12 \frac{e^2}{E_1} \tag{49}$$

where: $E_1 = \frac{1}{2} M_H v_1^2$.

Hence for the H^+- H collision, equation (45) yields

$$S^2 - \frac{2e^2}{E_1} S - \frac{e^4}{E_1^2} = 0$$

Which gives: $S(H^+ - H) \simeq 2.4 \frac{e^2}{E_1}$. (50)

Similarily, for the H-C collision we get:

$$S^2 - \frac{12e^2}{E_1} S - \frac{144 \ e^4}{E_1^2} = 0$$

which gives: $S(H\text{-}C) \simeq 7.4 \frac{e^2}{E_1}$. (51)

Hence the H^+ - H collision has the smallest distance of closest approach and hence equation (50) will establish the upper limit of validity of the classical approximation.

Consider first the restrictions imposed by equation (39). We require that: $\lambda << S$

or:

$$\frac{h}{\sqrt{2M_H E_1}} << 2.4 \frac{e^2}{E_1} \qquad \therefore E_1 << 1.45 \times 10^{+4} \text{ eV} . \tag{52}$$

Thus the wavelength considerations require $E_1 << 1.45 \times 10^4$ eV if our classical approximation is to be valid.

Consider the restrictions imposed by equation (43). We require that

$$D >> \frac{\hbar^2}{8M_H S^2}$$

or

$$D >> \frac{\hbar^2 E_1^2}{8M_H (2.4)^2 e^4} .$$

The binding energy of H_2^+ is 2.6 eV. Thus we get

$$E_1 << \sqrt{8M_H D} \left(\frac{2.4e^2}{\hbar}\right) \tag{53}$$

$$= 2.46 \times 10^{+3} \text{ eV}.$$

Hence equations (39) and (43) are satisfied if the energy of the incident proton beam is less than 1,000 electron volts. Thus the classical description of process (2) is valid in the 70 to 150 eV range where the experiment was performed.

III. EXPERIMENTAL APPARATUS

This experiment utilized experimental equipment that was designed, developed and assembled by many people. The overall apparatus as shown in Figure 5 was assembled and tested by Bush [5] and was first utilized satisfactorily by Smyth [6].

A reasonably mono-energetic beam of hydrogen ions ($\Delta E \sim 2$ eV) is produced in the Duoplasmatron, which was built and investigated by Carter [7]. The mass spectrometer constructed by Strohshal [8] is used to mass analyze the beam, and H^+ ions proceed on to the scattering chamber which contains the target gas, CH_4. The scattering cell is placed on the magnetic axis of a large cylindrical magnet at the position of maximum field. H_2^+ ions, produced by the collision of H^+ with CH_4, exit from the scattering cell and are focused by the axially symmetric non-uniform field of the focusing magnet to a point on the magnetic field axis, a distance Z_o from the scattering cell. The detector which is located at Z_o, is a continuous channel electron multiplier which was investigated by D'Arezzo [9].

A. THE DUOPLASMATRON

The duoplasmatron is shown in Figure 6. When filament power is at 35 watts and hydrogen is in the source, one has about .1 amp of electron emission from the filament. An arc voltage of 400 volts between the filament and the Z-electrode accelerates

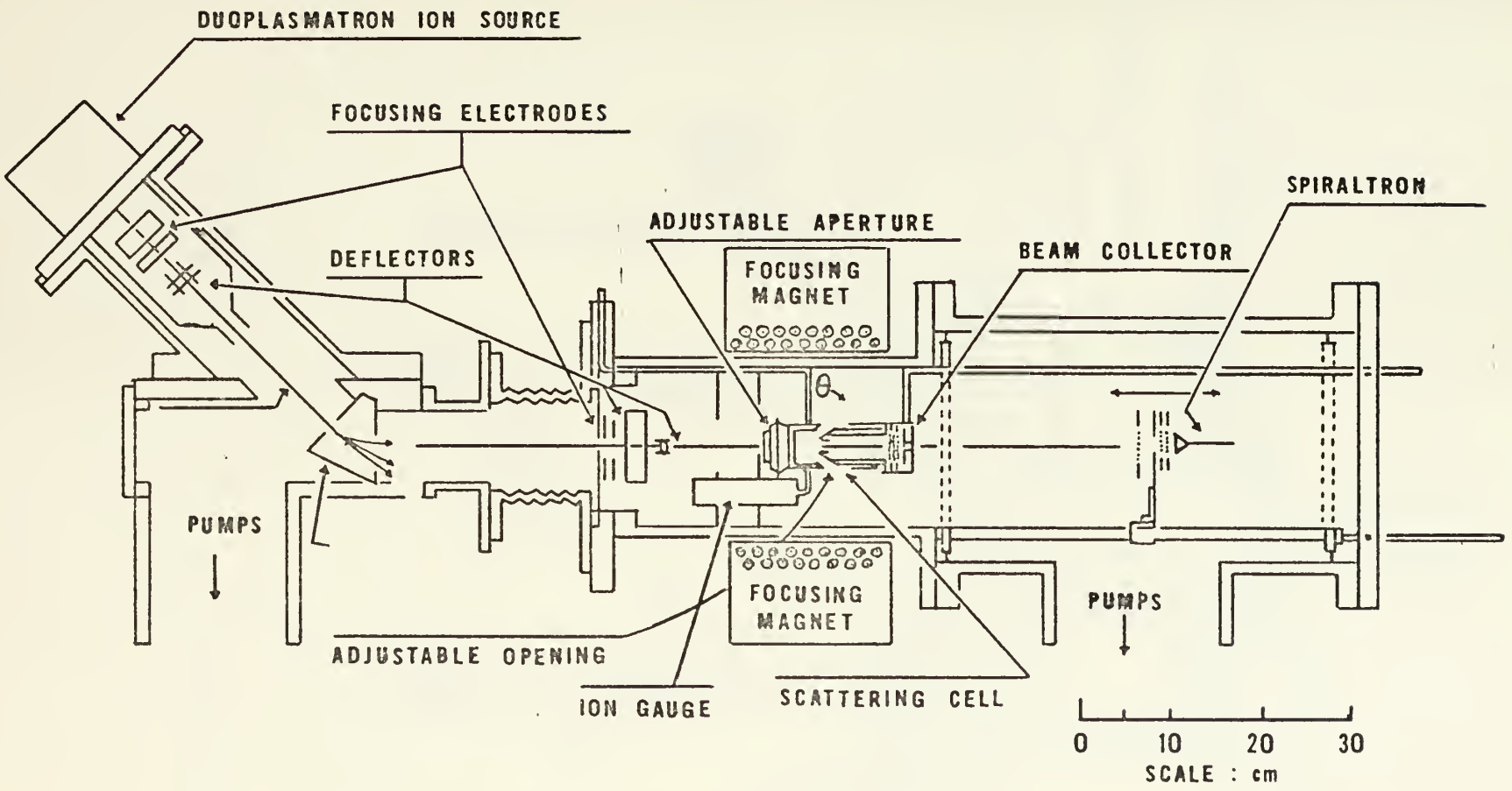

Fig. 5. Schematic of Experimental Apparatus

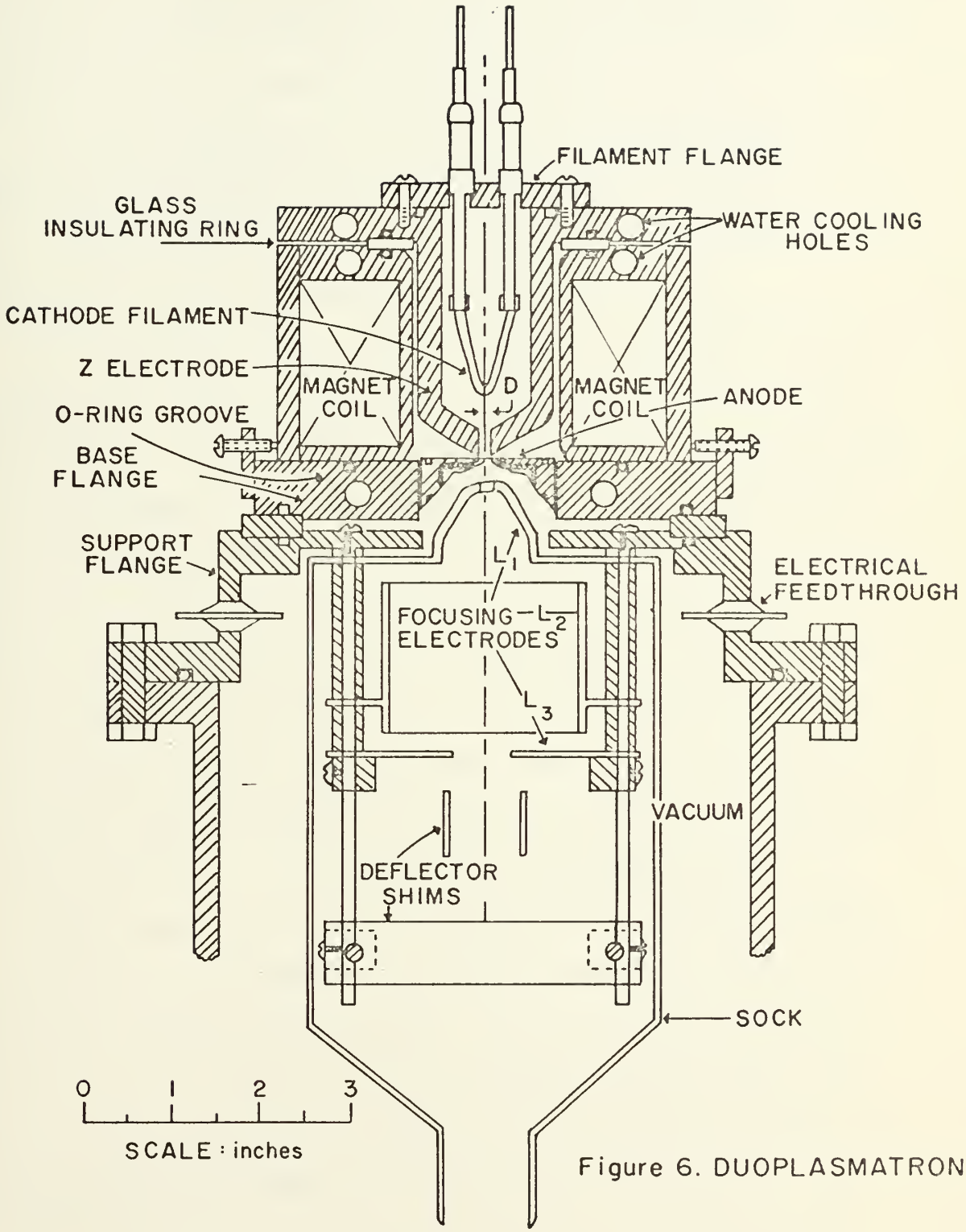

Figure 6. DUOPLASMATRON

these electrons through the hydrogen gas, ionizing the hydrogen and forming a plasma. Once the plasma has been formed, an arc current of 1 ampere can be sustained between the filament and the Z-electrode by a voltage of about 250 volts.

To extract the plasma, the positive arc voltage is switched from the Z-electrode to the anode, (see Figure 7) which is itself at a voltage E above ground. The energy of the hydrogen ion beam thus extracted will be (Ee) for singly charged ions.

To enhance the beam intensity a simple accel-decel system is employed. Figure 7 shows lens 1 at some arbitrary negative potential V. Thus the hydrogen ions are actually extracted from the duoplasmatron at an energy (V+E)e. A "sock" is fitted over the focusing and deflector lenses and attached to lens 1 so as to float at this negative potential V, and thus prevent the beam from "seeing" ground potential in this region. Thus the beam of hydrogen ions passes through the focusing and deflector lenses at an energy (V+E)e. Once the beam leaves the region of the "sock" it "sees" ground potential on the walls of the vacuum chamber and slows to an energy Ee and passes on to the mass analyzer.

This simple accel-decel system increased the beam intensity by a factor of 40. Thus we were able to obtain an analyzed beam of 100 eV protons (with diameter .5 cm at the scattering cell 80 cm from the source) which was slightly greater than 1×10^{-7} amps. Carter [7] has shown that the energy spread of the proton beam is less than 2.5%.

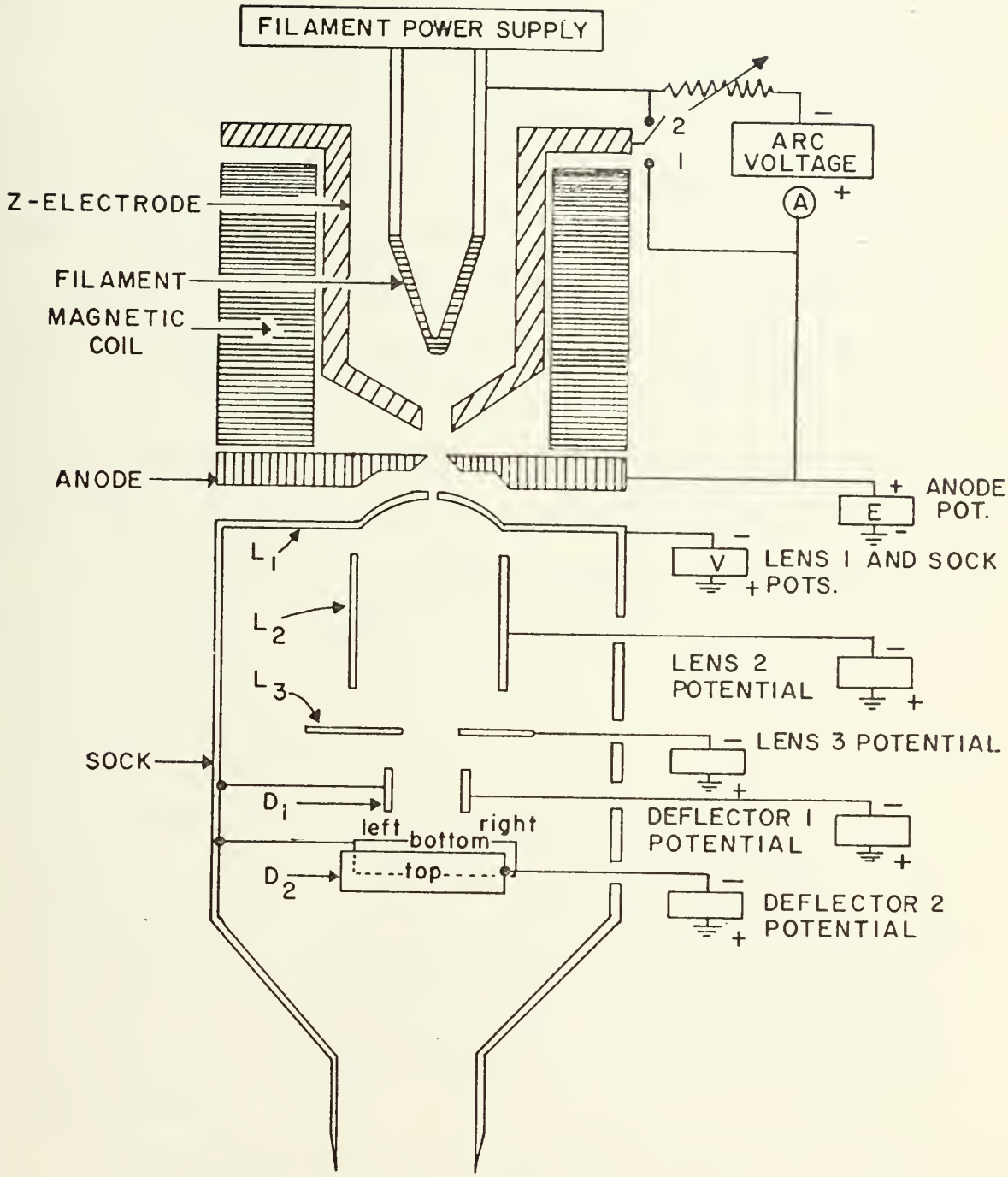

FIGURE 7.
CIRCUIT DIAGRAM FOR DUOPLASMATRON

B. THE MASS ANALYZER

The hydrogen ion beam is mass analyzed in the mass spectrometer constructed and calibrated by Strohsahl [8]. It employs a 45^{o} bending angle (see Figure 8) and has a resolution of $\frac{m}{\Delta m} = 40$ with beam transmission of about 90%.

Figure 9 shows the current through the mass analyzer magnet that will pass any particular species in the energy region from 50 to 650 volts. Hence 0.45 amps allows a 100 eV beam of protons to travel into the scattering cell, whereas the H_2^+ and H_3^+ are not bent enough by the magnetic field to be transmitted (see Figure 5.)

The mass analyzer is carefully aligned with the scattering cell and the detector, all of which are positioned on the axis of the focusing magnet.

C. THE SCATTERING CELL

The scattering cell, was designed and tested by Bush [1]. The target gas, methane, is bled into the scattering cell and is accurately controlled by a Variable Leak valve. The CH_4 gas is of research grade (purity 99.65%) and is maintained in the scattering cell at a pressure of approximately 10^{-3} torr as measured by the VG1A ion gauge.

The scattering cell has an adjustable aperture (generally set at .5 cm diameter) through which the proton beam passes before entering the scattering cell. In the cell the H^+ reacts with the CH_4 to form H_2^+ whose escape from the cell is limited by the

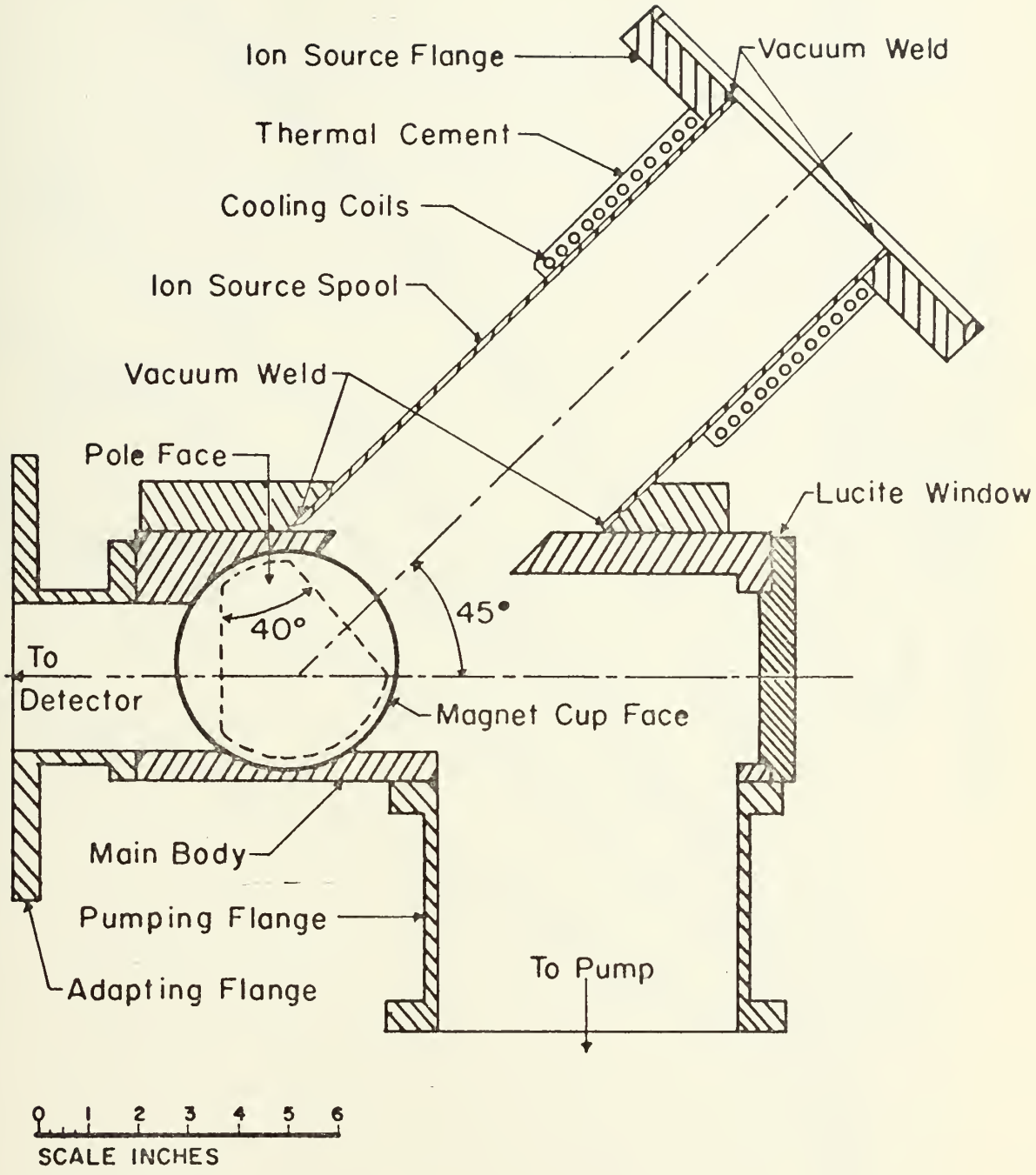

Figure 8. Schematic of Mass Spectrometer.

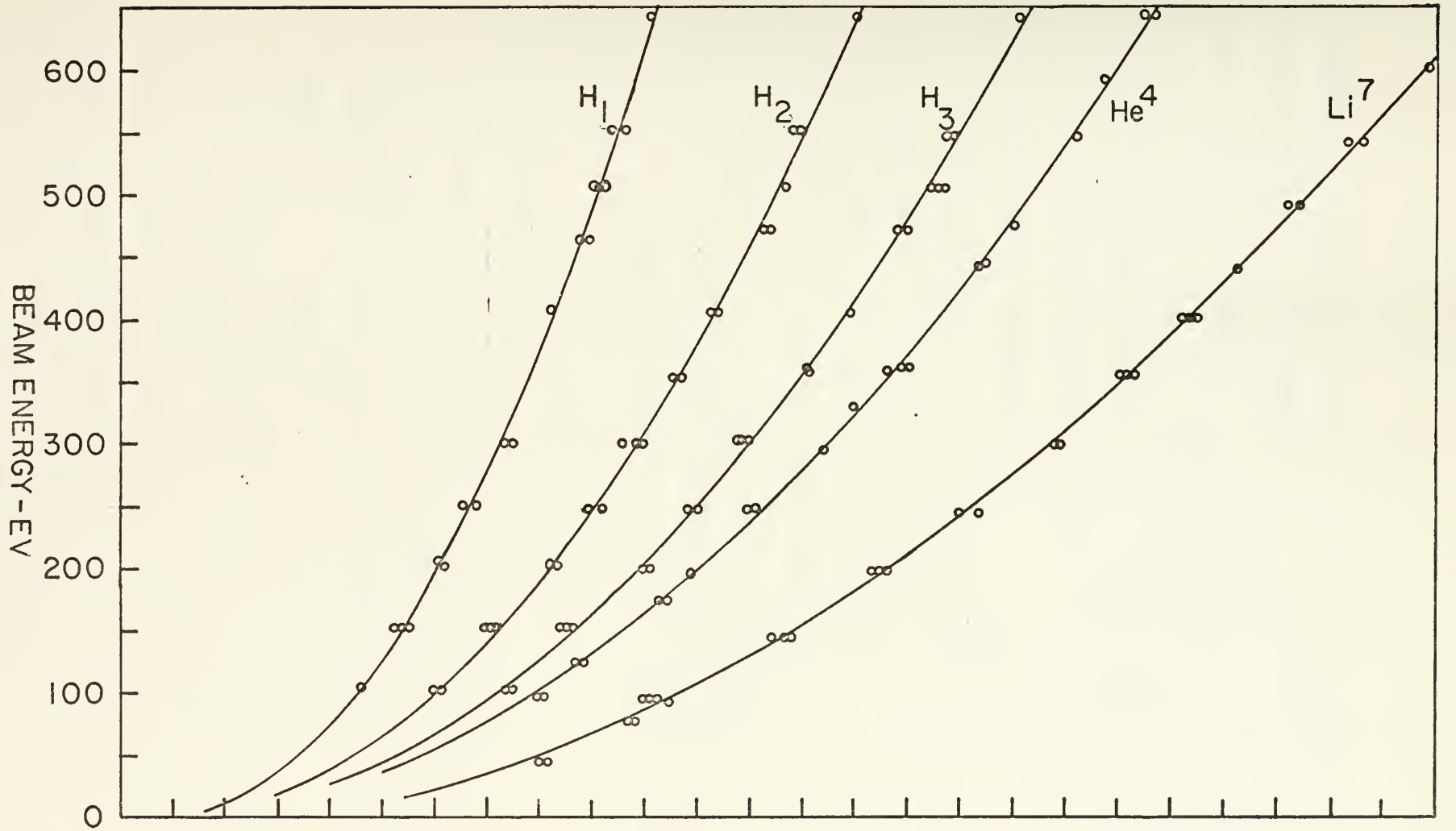

FIGURE 9

SPECTROMETER OPERATION CURVES

geometry of the exit opening. The exit is an annular opening of 360° reduced by support legs to about 290°, around the scattering cell, between the front and rear of the cell. The exist wall of the front section slopes upward at 49°, and the exit wall of the rear section slopes upward at 36°. By varying the separation of the front and rear sections of the scattering cell, the target thickness can be increased from 0 to 0.8 cm.

Two Keithly Model 410 Micro-micro Ammeters were used to measure the intensity of the incident beam at the front and rear of the scattering cell. The beam collector collects the unscattered beam (approximately 90%) and has three grids used to prevent slow ions from being collected and suppressing secondary electron emission. The beam collector assembly could be swung off axis allowing a clear path through the scattering cell for system alignment and detector calibration.

D. THE FOCUSING MAGNET

The magnetic field of the focusing magnet is non-uniform and axially symmetric and has the focusing property of bending the trajectories of charged particles so they follow a path similar to that shown in Figure 10.

If one considers the simpler case of an axially symmetric uniform magnetic field, it can be shown that the trajectory of a charged particle is a helix (see Ref. 5.) The particle will cross the field line on which it originated after one complete revolution. Then, as shown in Figure 10, particles of charge q leaving the

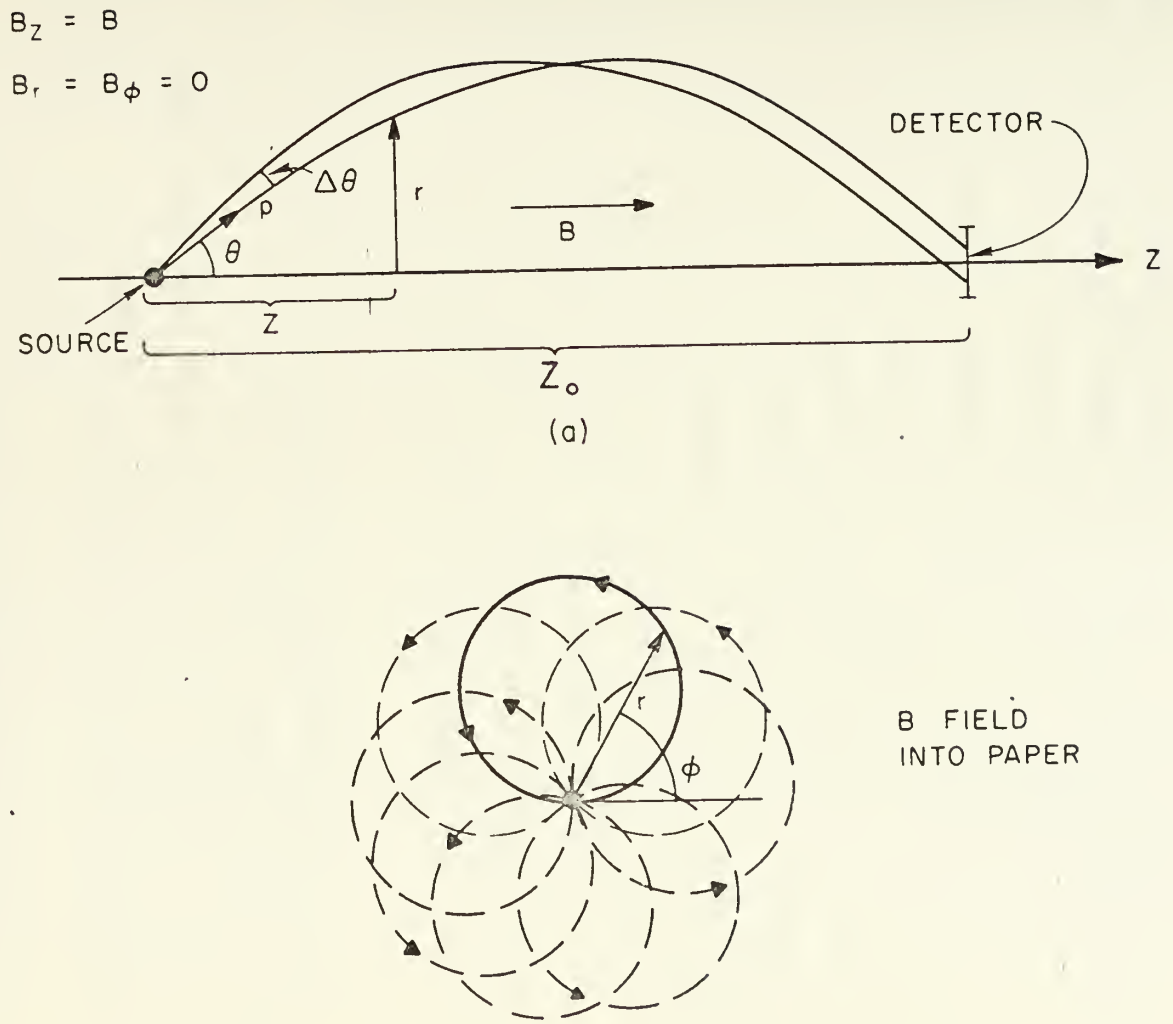

Figure 10. Orbit of Charged Particle in Uniform Magnetic Field

source (the scattering cell) with momentum p = mv at an angle θ will cross the magnetic axis at a distance Z_o given by

$$Z_o = \frac{2\pi p \cos \theta}{qB} \qquad (1)$$

where B is the magnetic field strength. Thus a detector located at Z_o will sense only those ions scattered out of the scattering cell placed at $Z = 0$ which have momentum p, charge q, and scattering angle θ. Now if one holds the detector fixed at Z_o and increases B then particles of larger p cos θ values will strike the detector. Alternately by holding B fixed and varying Z_o we can detect particles scattered from the source at different values of p cos θ. Now since equation 1 is independent of azimuthal angle ϕ, the entire 360^o can be observed at Z_o. In the particular configuration actually used in this experiment this is limited to 290^o by mechanical supports. Hence the solid angle is enhanced by a factor of approximately 300 over most conventional scattering experiments where $\Delta\theta \simeq 1^o$.

In our experimental apparatus the magnetic field is not uniform, as it is produced by a "thin" solenoid shown in Figure 5. This makes numerical integrations of the trajectory equations necessary. The results of numerical integrations for the H_2^+ ions are shown in Figure 11.

The magnetic field of the focusing magnet was measured by Kelly [10]. Figure 12 shows the axial component of the magnetic field on the magnetic axis. Figure 13 shows the values of the axial component of the magnetic field measured at various r and

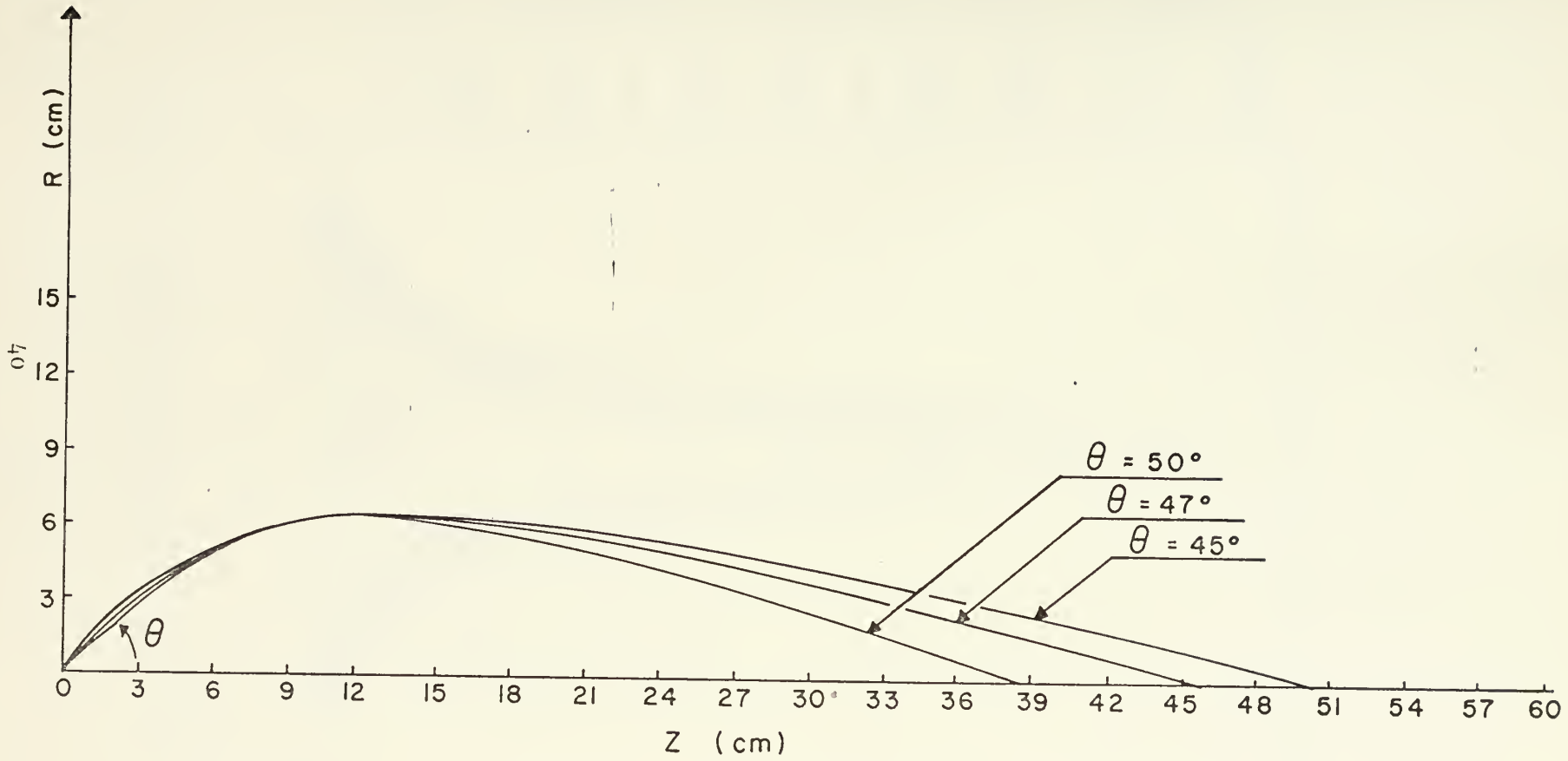

Figure 11. H_2^+ Trajectories in Field of Focusing Magnet

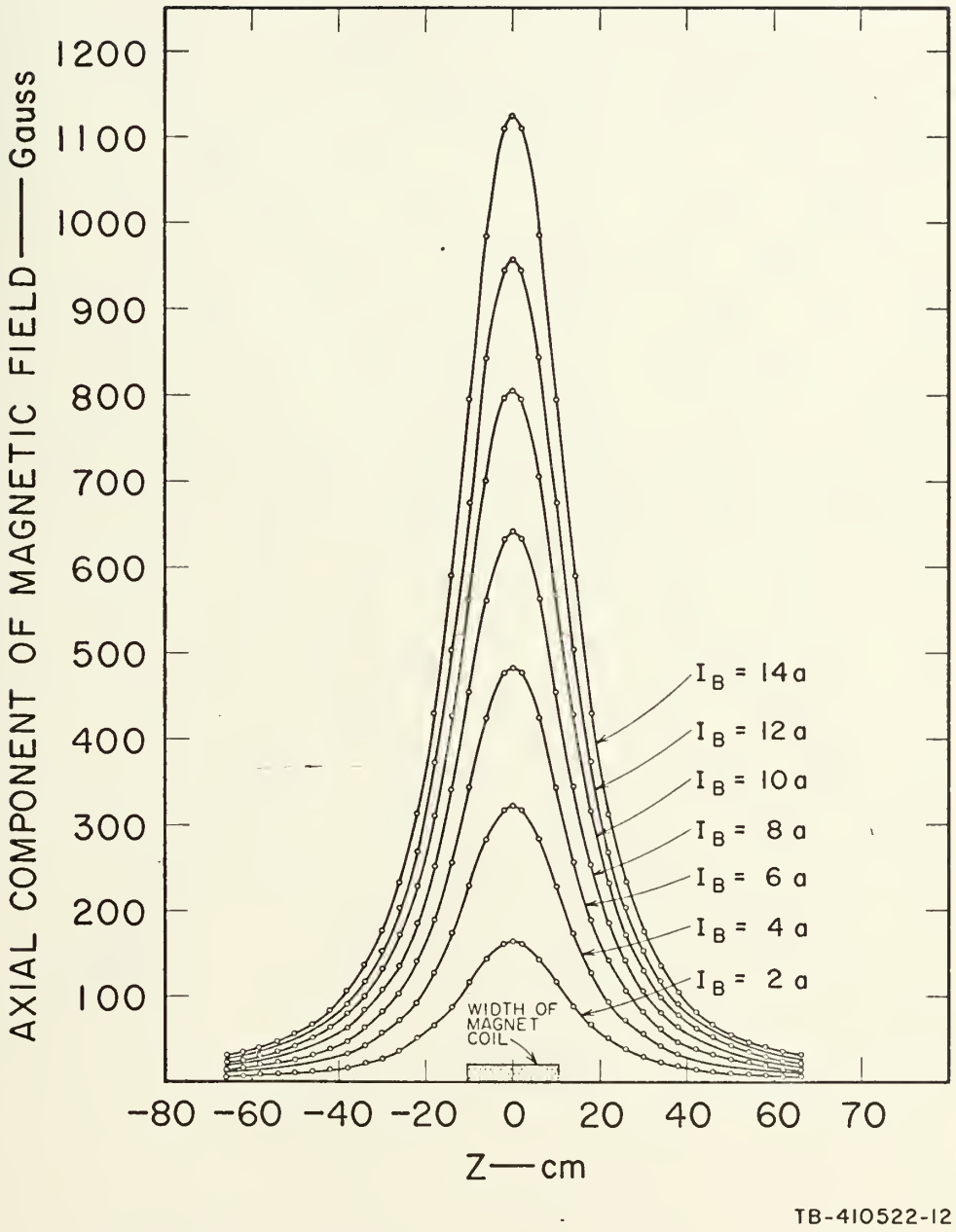

Figure 12 . Magnetic Field Strength at Various Distances Along the Magnetic Axis for Various Currents

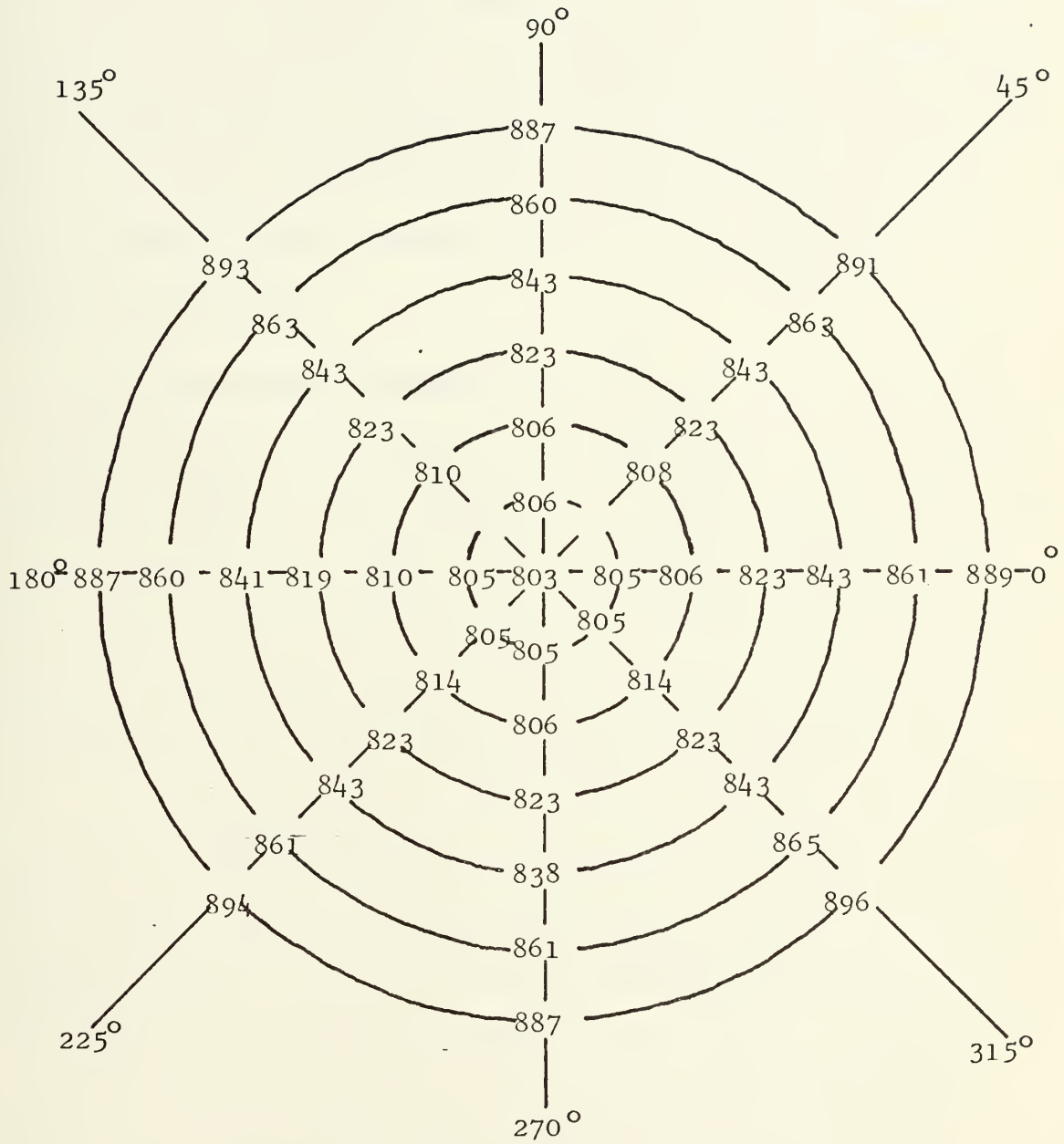

(Z_o = 0)

Fig.13. Axial Component of Magnetic Field at Z_o = 0 and at Various R and Ø Values

Ø values at the center of the coil. Figure 14a and b show the radial components of the magnetic field as measured with a Hall Probe (at Z_o = 34 cm) across the geometric axis of the coil, both vertically and horizontally. This demonstrates that the magnetic and geometric axis of the magnetic coil are aligned to with 0.1%. This allows use of the coil geometric axis and the coil center line as reference for alignment of the entire system along the magnetic field axis.

E. THE SCATTERED ION DETECTOR

The scattered ion detector was a continuous channel electron multiplier manufactured by Bendix Corp., Electro-Optics, Div. Its performance characteristics were investigated by D'Arezzo [9]. The geometry of the multiplier consists of a 0.2 cm diameter glass tube with an internal spiral structure coated with a semiconducting layer having a secondary electron emission coefficient greater than unity (see Figure 15.) The multiplier provides reproducable gains greater than 10^6 and is not adversely affected by the presence of the inhomogenous magnetic field produced by the focusing magnet. However the gain of the detector was noticably decreased for incident photon energies below 100 eV (see Ref. 9.) The output of the detector was fed to a Keithley Vibrating Capacitor Electrometer where the integrated current was measured.

F. SYSTEM ALIGNMENT

In order to detect particles scattered at a particular angle the detector must be placed on the focusing magnetic field axis

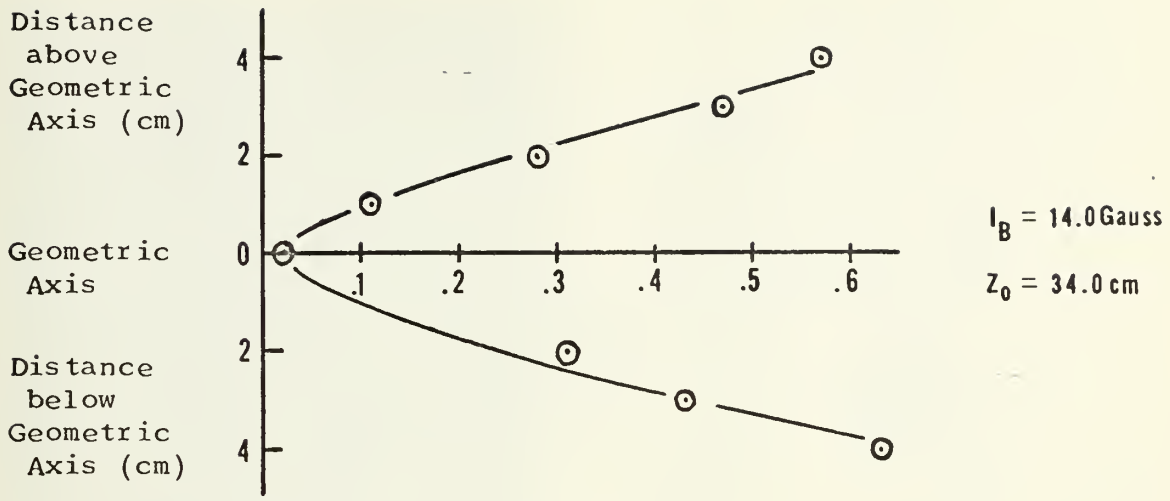

(a) I = 14.0 amp; Z = 34.0 cm
Radial Component of Magnetic Field Measured by Hall Probe above and below the Geometric Axis

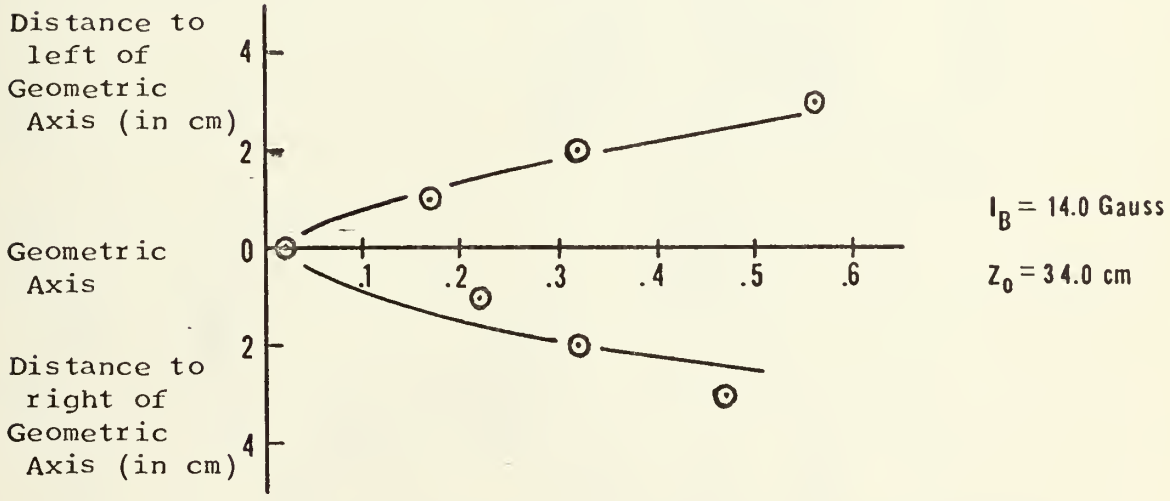

(b) I = 14.0 amp; Z = 34.0 cm
Radial Component of Magnetic Field Measured by Hall Probe to left and right of the Geometric Axis

Fig. 14. Radial Magnetic Field Components

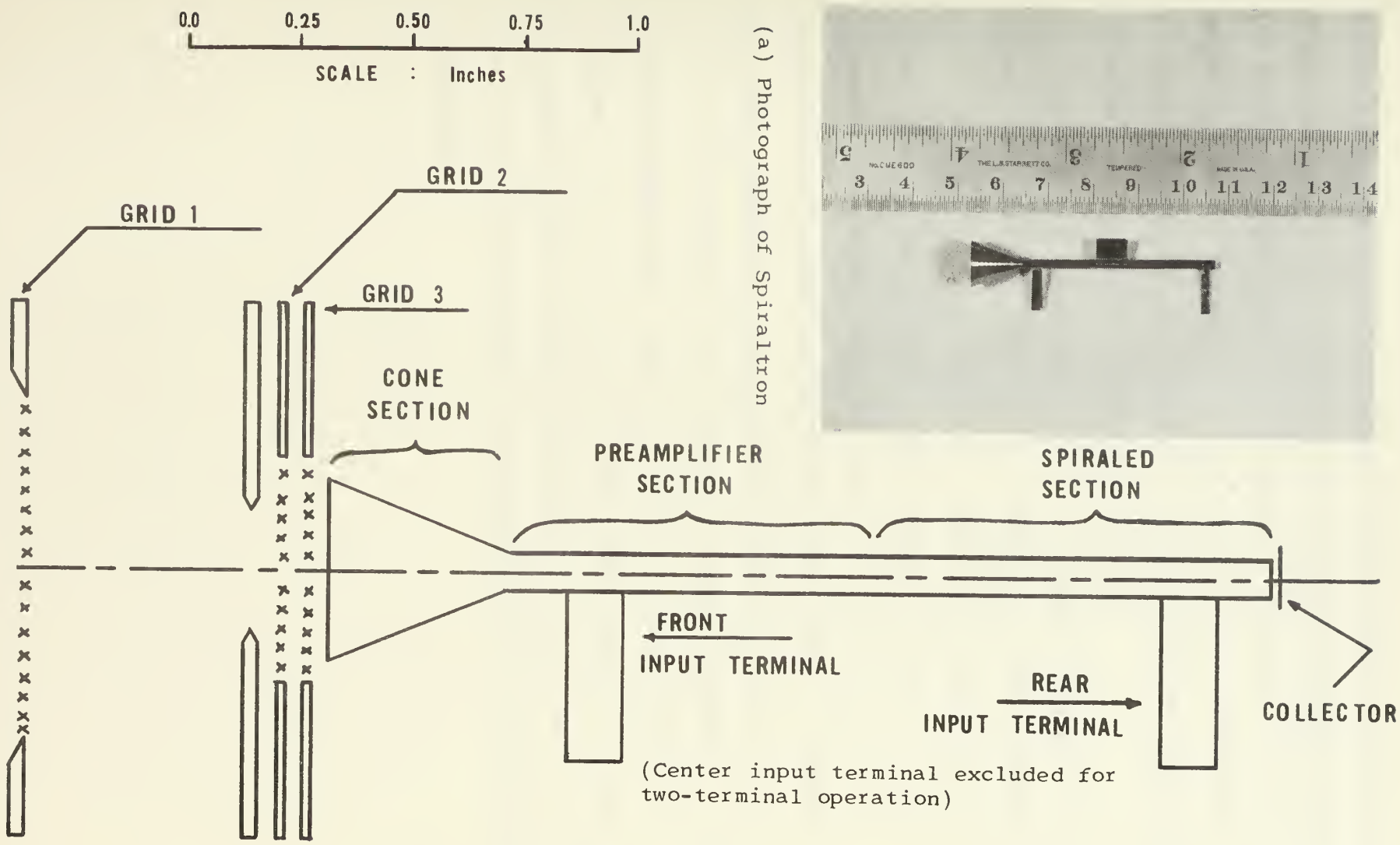

(b) Schematic of Spiraltron and Grid Assembly

Figure 15. Schematic of SEM

at the point Z where the scattered particles focus on the axis. The program SOLANG which calculates the intercept distance assumes that the scattering took place on the axis at the center of the focusing magnetic field. Therefore accuracy in the angle of scatter determination depends on the alignment of the scattering center and detector with respect to the magnetic field.

The geometric center line of the focusing magnet coil is used as the reference for aligning all components to the magnetic field axis. To perform this alignment, cross hairs were placed on either side of the magnetic spool to mark its axis. A small laboratory laser was then positioned so its beam lay on the magnetic axis established by the two cross hairs. The cross hairs were then removed and the line established by the laser beam was used as the reference for aligning all other components to the focusing magnet axis. The mass analyzer was constructed by Strohsahl [8], so that the ion beam, after analysis, travels down the geometric axis. Hence attaching cross hairs to the front and rear of the mass analyzer, it was adjusted into alignment with the laser beam.

IV. CALCULATION OF THE SCATTERING CROSS SECTION

A. THE SOLID ANGLE

In order to measure a differential scattering cross section, the solid angle subtended by the finite size detector must be known. This is $d\Omega = 2\pi \sin\theta \, d\theta$ for the axially symmetric case. The evaluation of $d\theta$ requires consideration of the various parameters affecting Z_o, the axis intercept distance. A functional relationship exists such that:

$$Z_o = f(E, \theta, B, \rho, \eta, C) \qquad (1)$$

where E = energy of incident ion

θ = angle of scatter

B = magnetic field

ρ = radial target displacement from the system axis

η = displacement of target atom from the scattering center along the system axis

C = constant for each reaction dependent upon mass ratios, in elastic energy losses, etc.

Differentiating expression (1) gives

$$\Delta Z_o = \left(\frac{\delta Z_o}{\delta E}\right)\Delta E + \left(\frac{\delta Z_o}{\delta \theta}\right)\Delta\theta + \left(\frac{\delta Z_o}{\delta B}\right)\Delta B + \left(\frac{\delta Z_o}{\delta \rho}\right)\Delta\rho + \left(\frac{\delta Z_o}{\delta \eta}\right)\Delta\eta + \left(\frac{\delta Z_o}{\delta C}\right)\Delta C \qquad (2)$$

In a given measurement ΔB and ΔC are zero. The remaining derivatives do not have known analytic expressions, so it is necessary to evaluate them numerically by varying E, θ, ρ and η. Bush, Cook,

Heinz, and Rodeback [11] estimate that $\Delta\rho$ and $\Delta\eta$ which are due to the finite volume of the scattering region affect $\Delta\theta$ by no more than 10%. If one approximates $\Delta\rho$ and $\Delta\eta$ as zero equation (2) becomes

$$\Delta\theta = \left(\frac{\delta\theta}{\delta Z_o}\right)\left[\Delta Z_o - \left(\frac{\delta Z_o}{\delta E}\right)\Delta E\right]. \qquad (3)$$

Consideration of a small (2%) energy spread indicates that the "effective" $\Delta\theta$ was not changed. The angular resolution of the apparatus was degraded in that not all particles scattered within $\Delta\theta$ of θ were collected, but this was compensated by the fact that some particles scattered outside of $\Delta\theta$ were collected. Hence the solid angle may be approximated by

$$d\Omega \simeq 2\pi \sin\theta \left|\frac{\delta\theta}{\delta Z_o}\right| \Delta Z_o \qquad (4)$$

where $\left|\frac{\Delta Z_o}{2}\right|$ is the maximum deviation of the trajectory intercept from Z_o that will still allow the particle to be collected in the detector. ΔZ_o can be calculated by considering the detector geometry and the angle θ (see Ref. 9.)

In the case of the non-uniform axially symmetric field, the procedure for the computation of the trajectories and the solid angles was essentially the same as for the uniform case except that the calculations were done numerically on an IBM 360-67 digital computer. The program for this calculation was originally written by Gagliano [12] but has subsequently been modified. A brief outline of the program is as follows:

1) The magnetic field along the axis is expressed as a 12^{th} order polynomial. This gives

$$B_z = (I) \sum_{1}^{13} C_n Z^{n-1} \qquad (5)$$

where I is the magnet current.

2) A vector potential is found from this polynomial.

3) The vector potential is combined with the Lorentz force equation to give a second order non-linear differential equation. This is, in turn, expressed as two simultaneous, first order differential equations which are integrated by the D H P G C Subroutine of the Scientific Subroutine Package for the IBM 360-67 computer. This provides the trajectory, Z_o and θ_o.

4) This procedure is done over a selected range of scattering angles, and a polynomial expression $\theta = f(Z_o)$ is generated.

5) ΔZ_o is calculated from θ_o and the detector geometry.

6) The solid angle can now be calculated as

$$d\Omega(\theta) = 2\pi \left(\frac{290}{360}\right) \sin\theta \left(\frac{d\theta}{dZ_o}\right) \Delta Z_o .$$

B. THE CROSS SECTION

Consider a beam of monoenergetic ions I_i incident on a target of N_t molecules. A detector located at an angle θ subtends solid angle $d\Omega(\theta)$. The number of particles scattered into the detector, N_s, is usually measured as a current I_s where:

$$I_s = N_s \, d\Omega(\theta)$$

The cross section is then defined as:

$$d\sigma(\theta) = \frac{I_s}{I_i N_t \, d\Omega(\theta)} . \qquad (6)$$

But I_s is magnified G times by the multiplier gain. Hence I_D, the actual detector current measured is

$$I_D = I_s \, G$$

Hence (6) becomes:

$$d\sigma(\theta) = \frac{I_D}{I_i G N_t \, d\Omega(\theta)}$$

But N_t, the number of target particles, is given by:

$$N_t = P_{sc} \rho t$$

Where P_{sc} = pressure of target gas in scattering cell in torr

$p = 3.536 \times 10^{16}$ particles/cm^3 torr

t = target length in cm

Hence we have:

$$d\sigma(\theta) = \frac{I_D}{I_i G P_{sc} \rho t \, d\Omega(\theta)} \text{ cm}^2 . \qquad (7)$$

Because of the construction of the scattering cell (see Section 3 of Chapter II), the target thickness depends on the scattering angle θ. Bush [5] has shown this relation to be:

$$t = S - \frac{2.54 \sin(36^\circ - \theta)}{\sin\theta} \quad \text{if } \theta < 36^\circ$$

$$t = S \quad \text{if } 36^\circ < \theta < 49^\circ \qquad (8)$$

$$t = S - \frac{2.0 \sin(\theta - 49^\circ)}{\sin\theta} \quad \text{if } 49^\circ < \theta$$

where S is the minimum separation of the front of the scattering cell from the rear of the scattering cell, (which is adjustable from outside the vacuum system.)

The differential cross section in the laboratory and Center of Mass coordinate systems is calculated by Computer Program CSVSZ (see Ref. 6) using equations (7) and (8) and the solid angle determined by the program SOLANG (see Ref. 6.)

V. EXPERIMENTAL RESULTS

The cross section for the formation of H_2^+ was measured at different angles of scattering by varying the detector distance Z while holding the magnet current I fixed. The cross section is expected to show a pronounced peak at an angle of scatter of 46.9° as discussed in Section B of Chapter II. Therefore the detector was swept through the range of scattering angles from 43° to 49°. This was repeated for three target gas pressures for each value of the energy of the incident proton beam. The energies investigated were 70, 100 and 150 electron volts. Measurements were attempted at 50 electron volts but were unsuccessful due to the decreasing detector gain as indicated by D'Arezzo [9]. The scattered data recorded at these energies are shown in Figures 16, 18 and 20 respectively. A pronounced peak exists in the 70 and 100 eV data, but the 150 eV data show no apparent peak in the cross section.

Analysis of the data was conducted in the following sequence. From the cross section measurements at each indident proton energy an average $\sigma(\theta)$ was computed and indicated by a solid angle. The background was indicated by a dotted line. The background was then subtracted out of the original data to produce the curves indicated by the solid curve in Figures 17 and 19. The effect of the angular resolution of the detector was considered and the actual curve

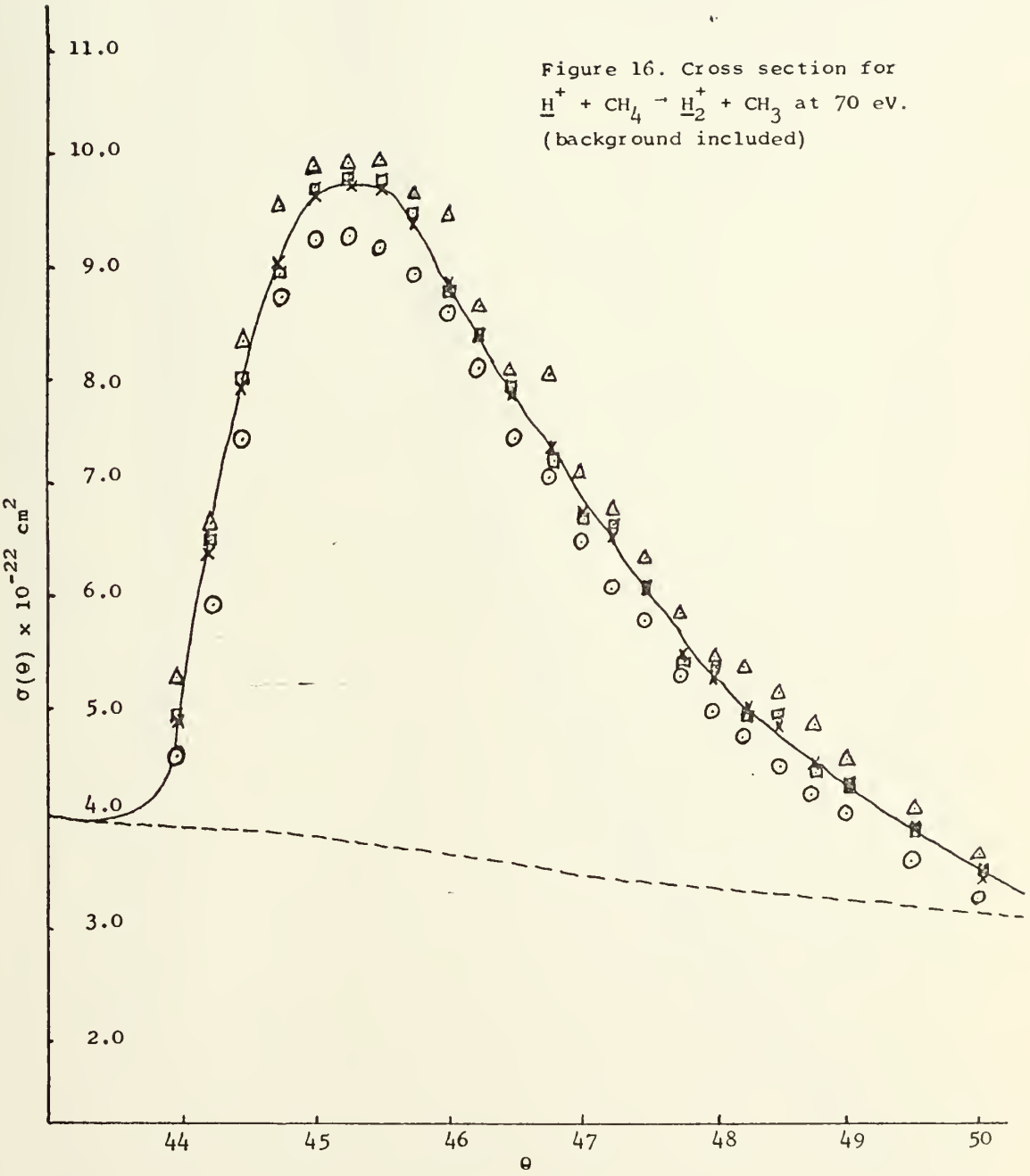

Figure 16. Cross section for $\underline{H}^+ + CH_4 \rightarrow \underline{H}_2^+ + CH_3$ at 70 eV. (background included)

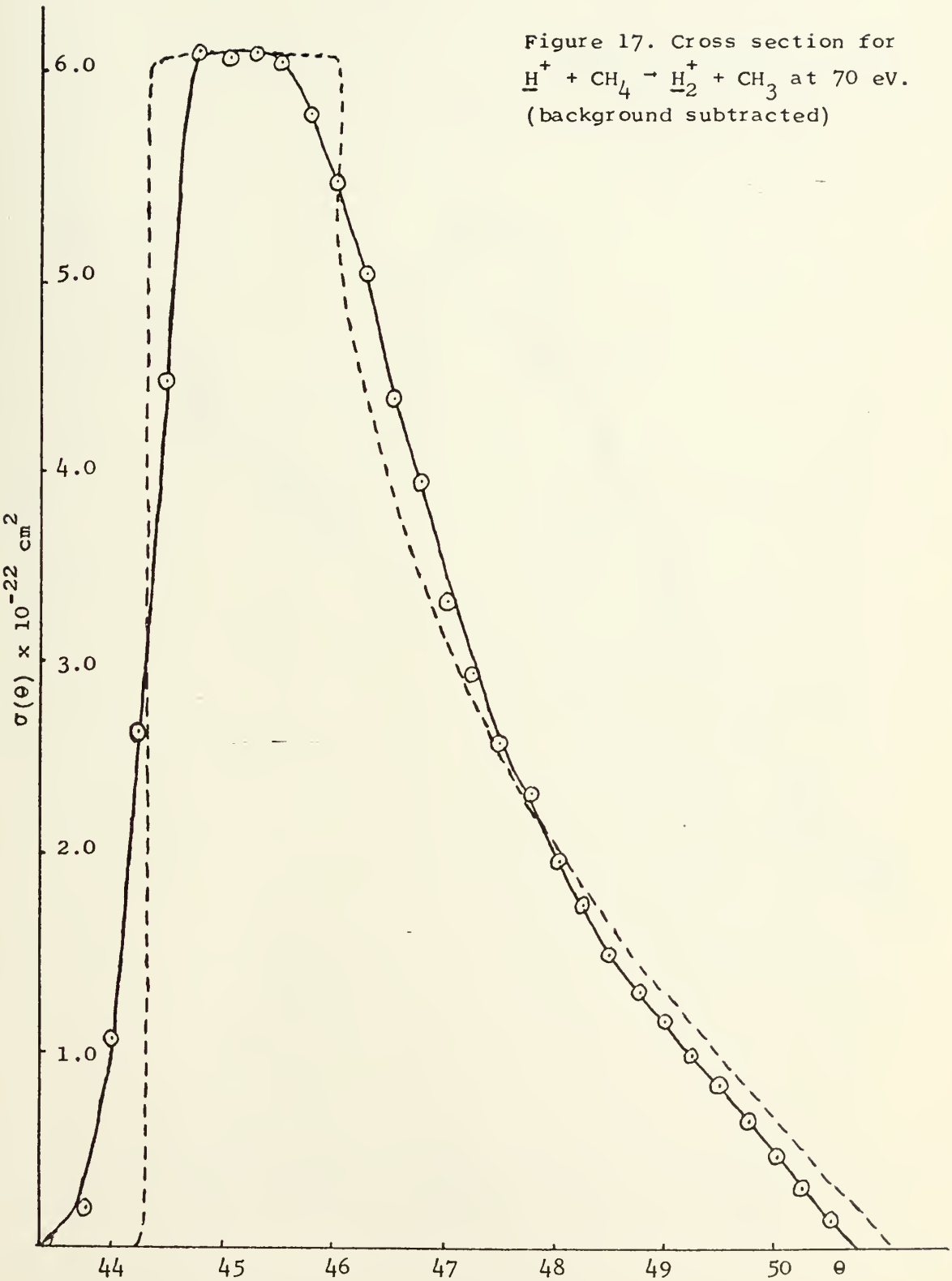

Figure 17. Cross section for $\underline{H}^+ + CH_4 \rightarrow \underline{H}_2^+ + CH_3$ at 70 eV. (background subtracted)

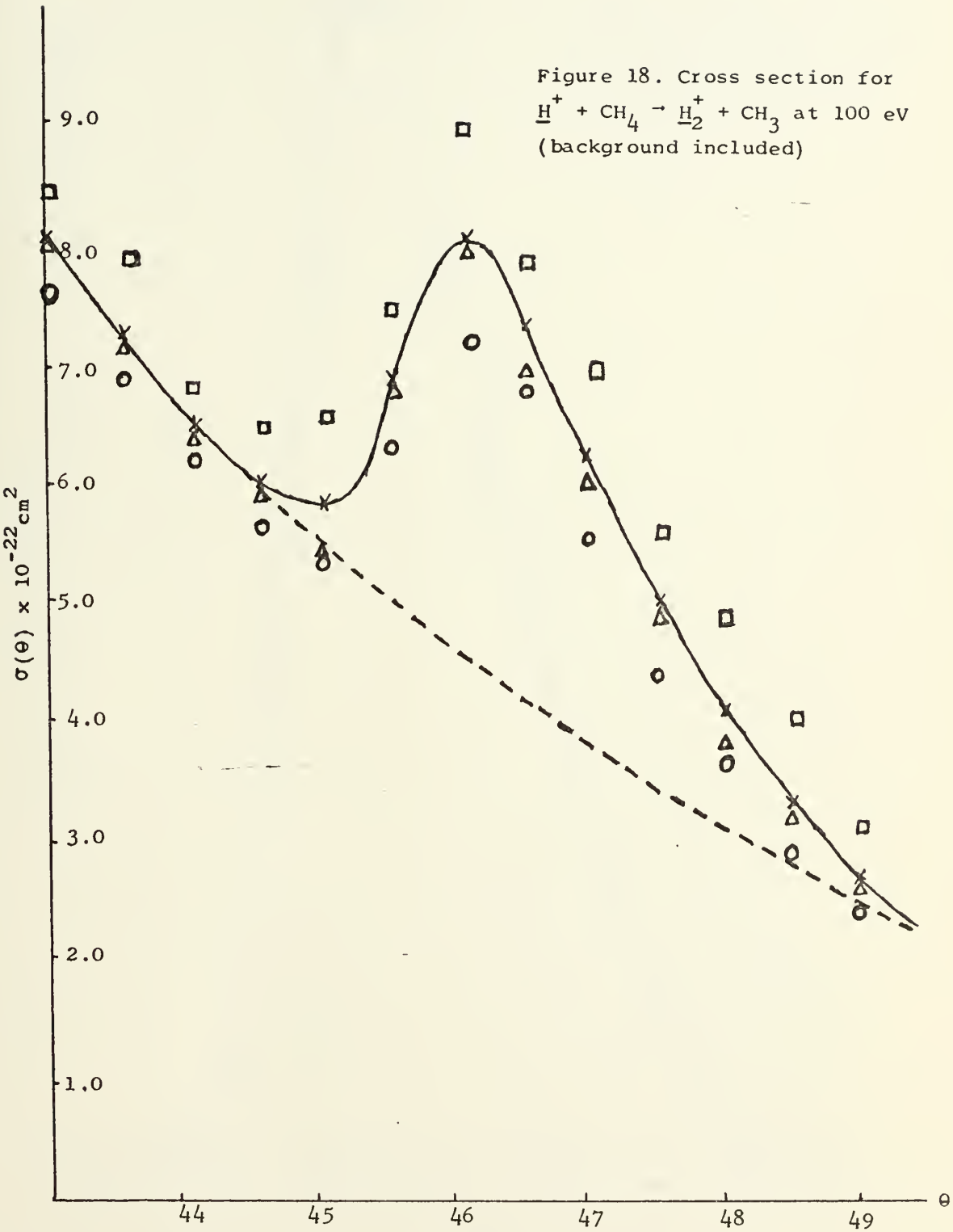

Figure 18. Cross section for $\underline{H}^+ + CH_4 \rightarrow \underline{H}_2^+ + CH_3$ at 100 eV (background included)

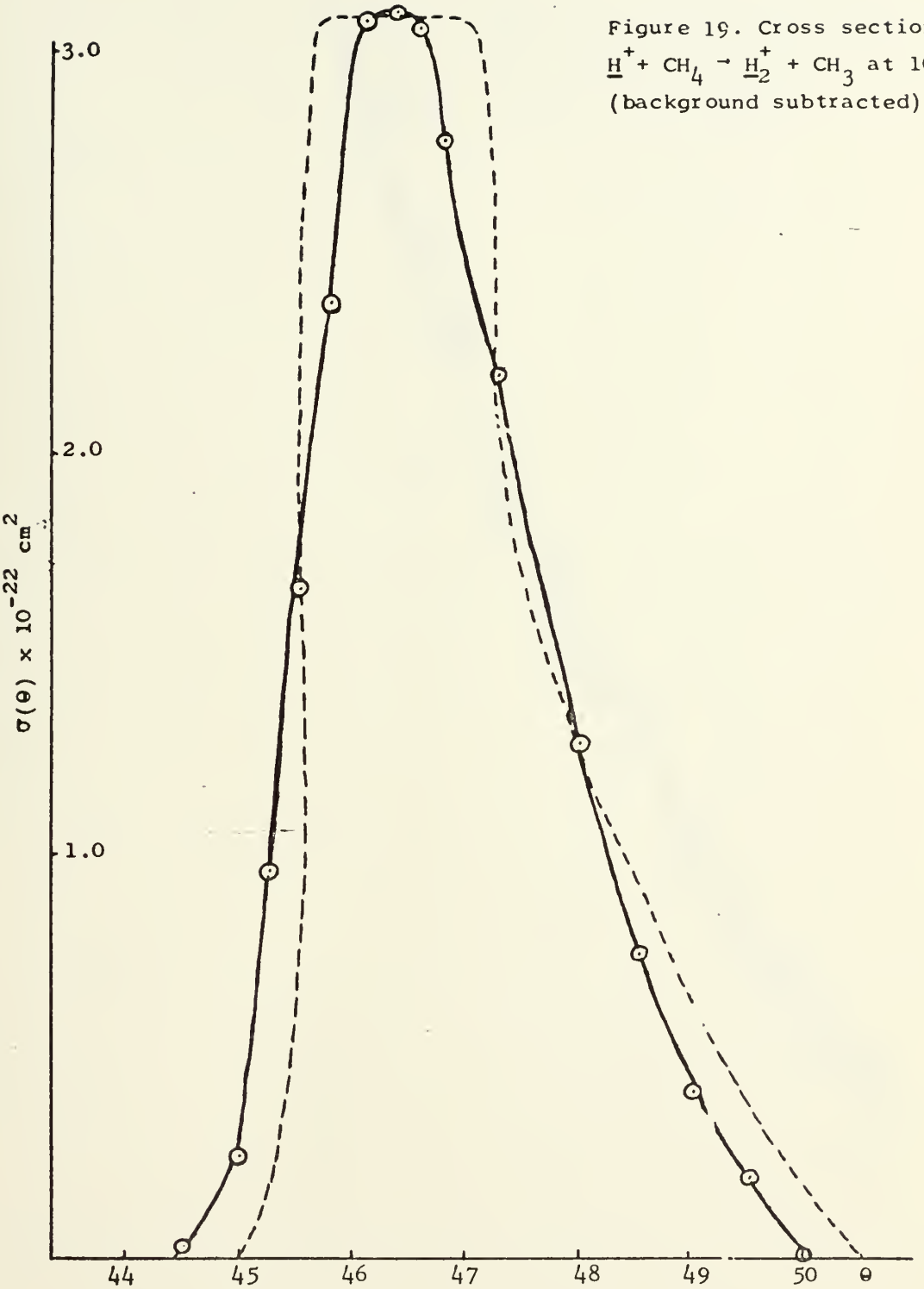

Figure 19. Cross section for $\underline{H}^+ + CH_4 \rightarrow \underline{H}_2^+ + CH_3$ at 100 eV (background subtracted)

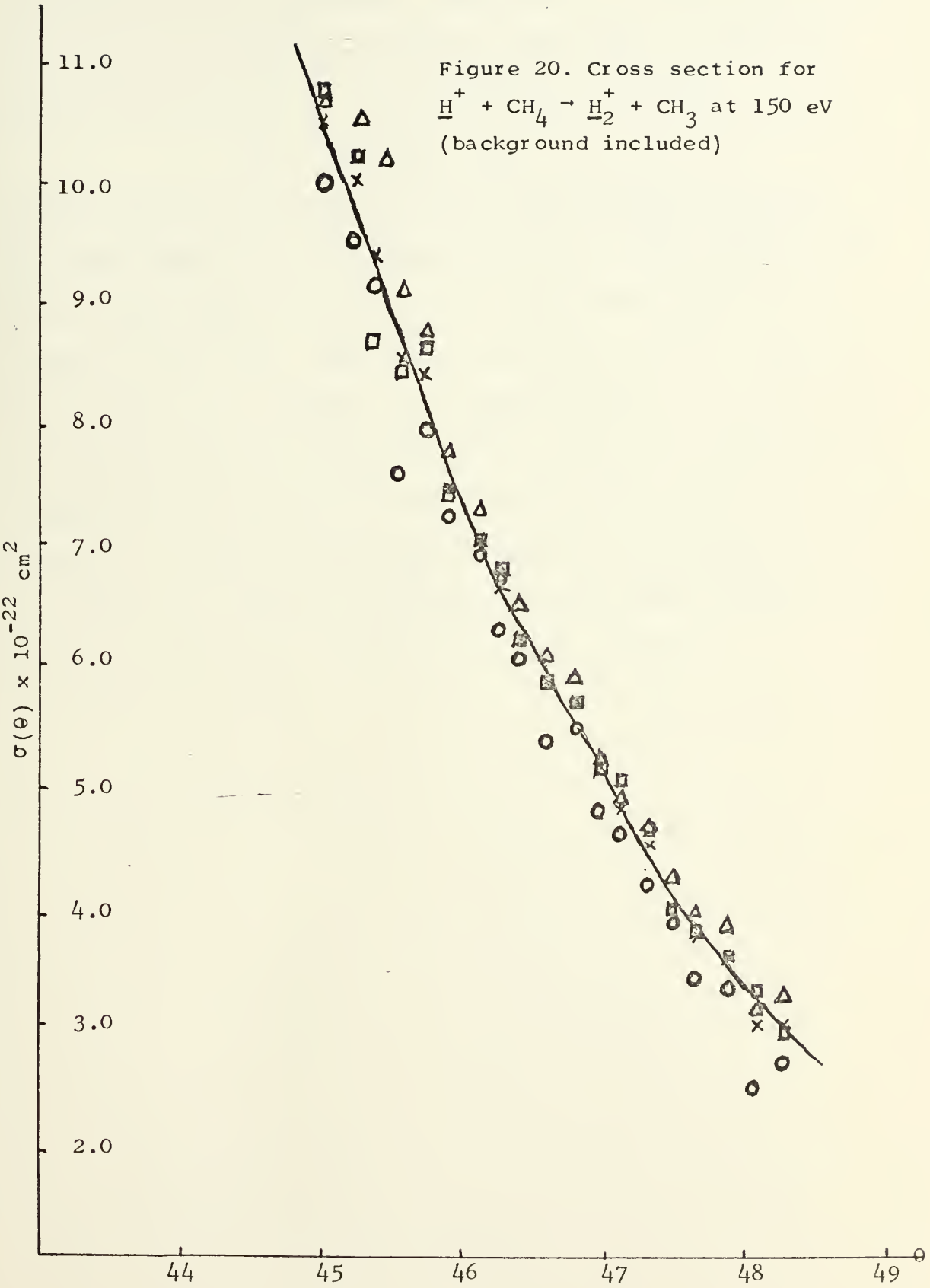

Figure 20. Cross section for $\underline{H}^+ + CH_4 \rightarrow \underline{H}_2^+ + CH_3$ at 150 eV (background included)

before detection was unfolded. These data are represented by the dotted curves in Figures 17 and 19. These peaks are then the actual cross sections for the rearrangement reaction:

$$\underline{H}^+ + CH_4 \rightarrow \underline{H}_2^+ + CH_3$$

as the energy of the incident proton varies from 70 to 100 eV. The peaks exhibit the same characteristics: a sharp leading edge at the lower angles, a flat top and a long decreasing tail extending to about 51^o. The 70 eV peak occurs at 45.2^o, and the 100 eV peak occurs at 46.3^o. The width of the peak at 70 eV is 1.7^o, and the width at 100 eV is 1.5^o. The energy dependence is compared to the theoretical cross section and to previous data in Figure 21. Curve (a) represents $\sigma(\theta)_{max}$, i.e. the magnitude of the flat top. Curve (b) represents the area under the flat top. Curve (c) represents the total area under the curve.

Figure 21. Energy dependence of cross section

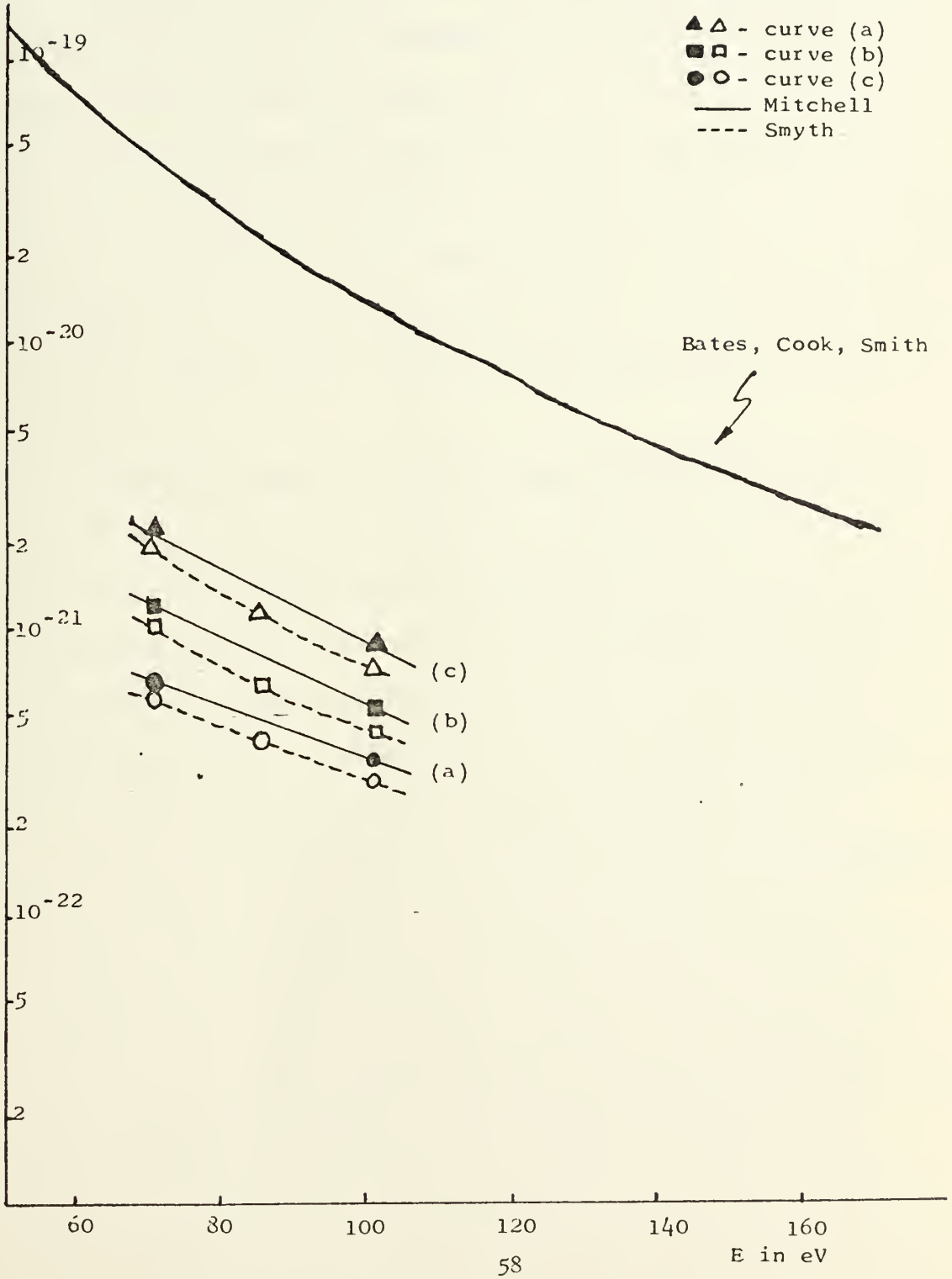

VI. CONCLUSION

The following observations as to the agreement between the experimental data and the predictions of the theory proposed by Bates, Cook and Smith are apparent:

(1) The predicted sharp peak is observed in the 70 and 100 eV data. The absence of the peak in the 150 eV data is not surprising since the magnitude of the cross section at 150 eV is $1.2 \times 10^{-27} cm^2$ as extrapolated from the experimental data. The 150 eV data on Figure 21 indicate that a peak of this magnitude cannot be observed.

(2) The theory proposed by Bates, Cook and Smith predicted the peak to occur at 46.9°. The peaks observed were at 45.2° and 46.3° with the larger angle corresponding to the higher energy. As the approximations made in the theory become more accurate as the energy increases, it would be expected that the peak in the experimental data would approach 46.9° as the energy is increased. This trend is consistent with the experimental data.

(3) The energy dependence of the cross section in the experimental data is similar to that predicted by the theory.

(4) Since the cross section predicted by Bates, Cook and Smith is an upper limit, it is reasonable to expect the experimental cross section to be lower. The observed cross section is indeed lower and in excellent agreement with the data by Smyth [6].

(5) The approximations made in the theory may decrease in validity at low energies. Therefore, one expects the peak to broaden as the energy decreases. This prediction is consistent with the experimental data.

It is felt that the preceeding facts along with the previous data by Smyth [6] constitute a verification of the ion-molecule rearrangement theory of Bates, Cook and Smith as applied to the formation of H_2^+ in the reaction

$$\underline{H}^+ + CH_4 \rightarrow \underline{H}_2^+ + CH_3 \ .$$

LIST OF REFERENCES

1. Bates, D.R.; Cook, C.J.; Smith, F.J.; "Classical Theory of Ion-Molecule Rearrangement Collisions at High Impact Energies", Proc. Phys. Soc. Vol. 83, p. 49, 1964.

2. Thomas, L.H.; "On the Capture of Electrons by Swiftly Moving Electrified Particles", Rog. Soc. Proc., Vol. A114, p. 561, 1927.

3. Byatt, W.J.; "Analytical Representation Hartree Potentials and Electron Scattering", Physical Review, Vol. 104, No. 5, Dec 1, 1956.

4. McDaniel, E.W.; "Collisional Phenomena in Ionized Gases", J. Wiley, 1964.

5. Bush, T.O.; "Large Angle Scattering of Lithium Ions by Helium Atoms", Unpublished Ph.D. Thesis, Naval Postgraduate School, Monterey, California, 1968.

6. Smyth, N.R.A.; "The Cross Section for the Formation of H_2^+ in the Reaction of Fast Protons with Methane", Unpublished Masters Thesis, Naval Postgraduate School, Monterey, California, 1969.

7. Carter, T.L.; "Ion Sources for the Production of Low Energy Beams", Unpublished Masters Thesis, Naval Postgraduate School, Monterey, California, 1968.

8. Strohsahl, G.H.; "Construction and Calibration of a Mass Spectrometer for the Analysis of Light Ions", Unpublished Masters Thesis, Naval Postgraduate School, Monterey, California, 1967.

9. D'Arezzo, R.A.; "Operating Characteristics of a Continuous Channel Electron Multiplier in a Magnetic Field", Unpublished Masters Thesis, Naval Postgraduate School, Monterey, California, 1970.

10. Kelly, P.J.; "Analogue Measurements of Charged Particle Trajectories in an Inhomogeneous Magnetic Field", Unpublished Masters Thesis, Naval Postgraduate School, Monterey, California, 1965.

11. Gagliano, R.A.; "Theoretical Trajectories of Charged Particles in an Inhomogeous Magnetic Field", Unpublished Masters Thesis, Naval Postgraduate School, Monterey, California, 1966.

12. Bush, T.O.; Heinz, O.; Rodeback, G.W.; Cook, C.J.; "Measurements of Large Angle Atomic Scattering Using Axially Symmetric Magnetic Fields", Submitted for Publication.

INITIAL DISTRIBUTION LIST

		No. of Copies
1.	Defense Documentation Center Cameron Station Alexandria, Virginia 22314	2
2.	Library Naval Postgraduate School Monterey, California 93940	1
3.	Dr. Otto Heinz Department of Physics Naval Postgraduate School Monterey, California 93940	1
4.	Dr. E.A. Milne Department of Physics Naval Postgraduate School Monterey, California 93940	1
5.	Dr. Charles C. Cook Stanford Research Institute (A220) Menlo Park, California 94025	1
6.	LT John T. Mitchell Hunters Point Naval Shipyard San Francisco, California	1

Blank

Page 64

DOCUMENT CONTROL DATA - R & D

(Security classification of title, body of abstract and indexing annotation must be entered when the overall report is classified)

1 ORIGINATING ACTIVITY (Corporate author)
Naval Postgraduate School
Monterey, California 93940

2a. REPORT SECURITY CLASSIFICATION
Unclassified

2b. GROUP

3 REPORT TITLE

Formation Cross Section of H_2^+ in the Reaction of Fast Protons and Methane

4 DESCRIPTIVE NOTES (Type of report and inclusive dates)
Master's Thesis; September 1970

5 AUTHOR(S) (First name, middle initial, last name)
John Thomas Mitchell, Jr.

6 REPORT DATE	7a. TOTAL NO. OF PAGES	7b. NO. OF REFS
September 1970	63	12

8a. CONTRACT OR GRANT NO.

b. PROJECT NO.

c.

d.

9a. ORIGINATOR'S REPORT NUMBER(S)

9b. OTHER REPORT NO(S) (Any other numbers that may be assigned this report)

10 DISTRIBUTION STATEMENT
This document has been approved for public release and sale; its distribution is unlimited.

11. SUPPLEMENTARY NOTES

12. SPONSORING MILITARY ACTIVITY
Naval Postgraduate School
Monterey, California 93940

13. ABSTRACT

The cross section for the formation of H_2^+ in the reaction $H^+ + CH_4 \rightarrow H_2^+ + CH_3$ was measured at scattering angles of 43^o to 49.5^o and incident proton energies of 70, 100 and 150 eV. For 150 eV the cross section showed no peak as a function of scattering angle. For 70 and 100 eV a pronounced peak was observed around a scattering angle of 46^o. The position of the peak tended toward the theoretical limit of 46.9^o as the incident proton energy was increased. The total cross section was 2.2×10^{-21} cm^2 at 70 eV and 8.1×10^{-22} at 100 eV. The angular position of the peak, the magnitude and the energy dependence of the cross section were in accordance with the classical theory of ion-molecule rearrangement collisions proposed by Bates, Cook and Smith.

14 KEY WORDS	LINK A		LINK B		LINK C	
	ROLE	WT	ROLE	WT	ROLE	WT
Atomic collision processes						
Ion-atom rearrangement collision						
Classical impulse approximation						
Capture process						
Axially symmatric magnetic field						
Cross section for H_2^+ formation						
Large angle scattering						
Continuous channel electron multiplier						

123143

Thesis
M6386 Mitchell
c.1 Formation cross section of H_2^+ in the reaction of fast protons and methane.